To appear in *Merging Processes in Clusters of Galaxies*, edited by L. Feretti, I. M. Gioia, and G. Giovannini (Dordrecht: Kluwer), in press (2001)

Chapter 1

THE PHYSICS OF CLUSTER MERGERS

Craig L. Sarazin
Department of Astronomy
University of Virginia
sarazin@virginia.edu

Abstract Clusters of galaxies generally form by the gravitational merger of smaller clusters and groups. Major cluster mergers are the most energetic events in the Universe since the Big Bang. Some of the basic physical properties of mergers will be discussed, with an emphasis on simple analytic arguments rather than numerical simulations. Semi-analytic estimates of merger rates are reviewed, and a simple treatment of the kinematics of binary mergers is given. Mergers drive shocks into the intracluster medium, and these shocks heat the gas and should also accelerate nonthermal relativistic particles. X-ray observations of shocks can be used to determine the geometry and kinematics of the merger. Many clusters contain cooling flow cores; the hydrodynamical interactions of these cores with the hotter, less dense gas during mergers are discussed. As a result of particle acceleration in shocks, clusters of galaxies should contain very large populations of relativistic electrons and ions. Electrons with Lorentz factors $\gamma \sim 300$ (energies $E = \gamma m_e c^2 \sim 150$ MeV) are expected to be particularly common. Observations and models for the radio, extreme ultraviolet, hard X-ray, and gamma-ray emission from nonthermal particles accelerated in these mergers are described.

1. INTRODUCTION

Major cluster mergers are the most energetic events in the Universe since the Big Bang. Cluster mergers are the mechanism by which clusters are assembled. In these mergers, the subclusters collide at velocities of $\sim$2000 km/s, releasing gravitational binding energies of as much as $\gtrsim 10^{64}$ ergs. During mergers, shocks are driven into the intracluster medium. In major mergers, these hydrodynamical shocks dissipate energies of $\sim 3 \times 10^{63}$ ergs; such shocks are the major heating source for the X-ray emitting intracluster medium. The shock velocities in merger

shocks are similar to those in supernova remnants in our Galaxy, and we expect them to produce similar effects. Mergers shocks should heat and compress the X-ray emitting intracluster gas, and increase its entropy. We also expect that particle acceleration by these shocks will produce relativistic electrons and ions, and these can produce synchrotron radio, inverse Compton (IC) EUV and hard X-ray, and gamma-ray emission.

In this chapter, I will review some of the basic physics of cluster mergers. As later chapters discuss the optical, X-ray, and radio observations of mergers, I will concentrate of theoretical issues. Also, because later chapters discuss simulations of cluster mergers and of large scale structure, I will mainly discuss analytical or semi-analytical aspects of cluster mergers. In § 2.1, semi-analytic estimates of merger rates based on Press-Schechter theory are reviewed. Some simple estimates of the kinematics of binary cluster mergers are given in § 2.2. The thermal effects of merger shocks are discussed in § 3, with an emphasis on determining the physical conditions in mergers from X-ray observations of temperatures and densities. Many clusters and groups contain cooling flow cores. During a merger, these cool cores will interact hydrodynamically with the hotter, more diffuse intracluster gas (§ 4). This can lead to the disruption of the cooling flow core, as discussed in § 4.1. Recently, the Chandra X-ray Observatory has detected a number of "cold fronts" in merging clusters, which apparently are cool cores moving through hot, shock heated, diffuse cluster gas (§ 4.2). Relativistic particles may be accelerated or reaccelerated in merger shocks or turbulence generated by mergers. The nonthermal effects of mergers are discussed in § 5. The resulting radio, extreme ultraviolet, hard X-ray, and gamma-ray emission is described.

2. BASIC MERGER RATES AND KINEMATICS

2.1. ESTIMATES OF MERGER RATES

The rates of cluster mergers as a function of the cluster masses and redshift can be estimated using a simple formalism originally proposed by Press & Schechter (1974, hereafter PS), and developed in more detail by Bond et al. (1991) and Lacey & Cole (1993), among others. Comparisons to observations of clusters and to numerical simulations show that PS provides a good representation of the statistical properties of clusters, if the PS parameters are carefully selected (e.g., Lacey & Cole 1993; Bryan & Norman 1998). This formalism assumes that galaxies and clusters grow by the gravitational instability of initially small amplitude gaussian density fluctuations generated by some process in the early

Universe. The fluctuation spectrum is assumed to have larger amplitudes on smaller scales. Thus, galaxies and clusters form hierarchically, with lower mass objects (galaxies and groups of galaxies) forming before larger clusters. These smaller objects then merge to form clusters.

In the extended PS formalism, the density fluctuations in the Universe are smoothed on a variety of mass scales. Regions are assumed to collapse when their density exceeds a critical value, which is usually taken to be the density for the collapse for an isolated, spherical mass concentration of the same mass. If one smooths the density fluctuations in some region on a variety of mass scales, the average density may exceed the critical density for collapse on a variety of different mass scales. The assumption of the extended PS formalism is that material is associated with the largest mass scale for which collapse has occurred, and that smaller mass scales have merged into the larger object. With these assumptions, the PS formalism allows one to estimate the abundance of clusters as a function of their mass, and the rates at which clusters merge.

Let $n(M,z)dM$ be the comoving number density of clusters with masses in the range M to $M+dM$ in the Universe at a redshift of z. According to PS, the differential number density is given by

$$n(M,z)\,dM = \sqrt{\frac{2}{\pi}}\,\frac{\overline{\rho}}{M^2}\,\frac{\delta_c(z)}{\sigma(M)}\,\left|\frac{d\,\ln\,\sigma(M)}{d\,\ln\,M}\right|\,\exp\left[-\frac{\delta_c^2(z)}{2\sigma^2(M)}\right]\,dM\,, \quad (1)$$

where $\overline{\rho}$ is the current mean density of the Universe, $\sigma(M)$ is the current rms density fluctuation within a sphere of mean mass M, and $\delta_c(z)$ is the critical linear overdensity for a region to collapse at a redshift z.

In Cold Dark Matter models, the initial spectrum of fluctuations can be calculated for various cosmologies (Bardeen et al. 1985). Over the range of scales covered by clusters, it is generally sufficient to consider a power-law spectrum of density perturbations, which is consistent with these CDM models:

$$\sigma(M) = \sigma_8\,\left(\frac{M}{M_8}\right)^{-\alpha}\,, \quad (2)$$

where σ_8 is the present day rms density fluctuation on a scale of 8 h^{-1} Mpc, $M_8 = (4\pi/3)(8\,h^{-1}\,\mathrm{Mpc})^3\bar{\rho}$ is the mass contained in a sphere of radius 8 h^{-1} Mpc, and the Hubble constant is $H_0 = 100\,h$ km s^{-1} Mpc^{-1}. The exponent α is given by $\alpha = (n+3)/6$, where the power spectrum of fluctuations varies with wavenumber k as k^n. The observations are generally reproduced with values of $-2 \lesssim n \lesssim -1$, leading to $1/6 \lesssim \alpha \lesssim 1/3$. The normalization of the power spectrum and overall present-day abundance of clusters is set by σ_8. The observed present-day abundance

of clusters leads to $\sigma_8 \approx 0.6\Omega_0^{-1/2}$, where $\Omega_0 \equiv \bar{\rho}/\rho_c$ is the ratio of the current mass density to the critical mass density, $\rho_c = 3H_0^2/(8\pi G)$ (e.g., Bahcall & Fan 1998).

The evolution of the density of clusters is encapsulated in the critical over-density $\delta_c(z)$ in equation (1). In general, $\delta_c(z) \propto 1/D(t)$, where $D(t)$ is the growth factor of linear perturbations as a function of cosmic time t (see Peebles [1980], § 11 for details). Expressions for the $\delta_c(z)$ in different cosmological models are:

$$\delta_c(z) = \begin{cases} \frac{3}{2}D(t_0)\left[1+\left(\frac{t_\Omega}{t}\right)^{\frac{2}{3}}\right] & (\Omega_0 < 1\,,\ \Omega_\Lambda = 0) \\ \frac{3(12\pi)^{\frac{2}{3}}}{20}\left(\frac{t_0}{t}\right)^{\frac{2}{3}} & (\Omega_0 = 1\,,\ \Omega_\Lambda = 0) \\ \frac{D(t_0)}{D(t)}\left(\frac{3(12\pi)^{\frac{2}{3}}}{20}\right)(1+0.0123\ \log\Omega_z) & (\Omega_0+\Omega_\Lambda = 1) \end{cases} \tag{3}$$

Here, Ω_Λ gives the contribution due to a cosmological constant Λ, where $\Omega_\Lambda \equiv \Lambda/(3H_0^2)$. For the open model ($\Omega_0 < 1$, $\Omega_\Lambda = 0$), $t_\Omega \equiv \pi H_0^{-1}\Omega_0 (1-\Omega_0)^{-\frac{3}{2}}$ represents the epoch at which a nearly constant expansion takes over and no new clustering can occur. The growth factor can be expressed as

$$D(t) = \frac{3\ \sinh\eta\,(\sinh\eta - \eta)}{(\cosh\eta - 1)^2} - 2 \tag{4}$$

where η is the standard parameter in the cosmic expansion equations (Peebles 1980, eqn. 13.10)

$$\begin{aligned} \tfrac{1}{1+z} &= \tfrac{\Omega_0}{2(1-\Omega_0)}\,(\cosh\eta - 1)\ , \\ H_0 t &= \tfrac{\Omega_0}{2(1-\Omega_0)^{\frac{3}{2}}}\,(\sinh\eta - \eta)\ . \end{aligned} \tag{5}$$

The solution for δ_c in the Einstein-deSitter model ($\Omega_0 = 1$, $\Omega_\Lambda = 0$) can be obtained from the open model solution by the limit $t_\Omega/t \to \infty$. The expression for δ_c in the flat model ($\Omega_0 + \Omega_\Lambda = 1$) is an approximation given by Kitayama & Suto (1996). Here Ω_z is the value of the mass density ratio Ω at the redshift z,

$$\Omega_z = \frac{\Omega_0\,(1+z)^3}{\Omega_0\,(1+z)^3 + \Omega_\Lambda}\,. \tag{6}$$

In this model the growth factor can be written as

$$D(x) = \frac{(x^3+2)^{1/2}}{x^{3/2}} \int_0^x x^{3/2}\,(x^3+2)^{-3/2} dx \tag{7}$$

(Peebles 1980, eqn. 13.6) where $x_0 \equiv (2\Omega_\Lambda/\Omega_0)^{1/3}$ and $x = x_0/(1+z)$.

The PS formalism also provides estimates of the merger history, rates, and probabilities for clusters. For example, the probability that a cluster with a mass M_0 at the present time t_0 had a progenitor with a mass of M at an earlier time $t < t_0$ is given by

$$\frac{dp}{dM}(M,t|M_0,t_0) = \frac{\delta_c(t)-\delta_c(t_0)}{\sqrt{2\pi}\left[\sigma^2(M)-\sigma^2(M_0)\right]^{3/2}}\left(\frac{M_0}{M}\right)\left|\frac{d\,\sigma^2(M)}{d\,M}\right| \exp\left\{-\frac{\left[\delta_c(t)-\delta_c(t_0)\right]^2}{2\left[\sigma^2(M)-\sigma^2(M_0)\right]}\right\}. \quad (8)$$

Similarly, the probability that a cluster of mass M undergoes a merger with cluster of mass ΔM per unit time is given by

$$\frac{d^2p}{d\Delta M\,dt} = \sqrt{\frac{2}{\pi}}\,\frac{\delta_c(z)}{\sigma(M')}\left|\frac{d\,\ln\delta_c(z)}{dt}\right|\left|\frac{d\,\ln\,\sigma(M')}{d\,M'}\right|\left[1-\frac{\sigma^2(M')}{\sigma^2(M)}\right]^{-3/2} \times\exp\left\{-\frac{\delta_c^2(z)}{2}\left[\frac{1}{\sigma^2(M')}-\frac{1}{\sigma^2(M)}\right]\right\}, \quad (9)$$

where $M' = M + \Delta M$.

These probability distributions can be used to make Monte Carlo simulations of the merger histories which produced clusters of a various masses at present. Figure 1.1 shows one such "merger tree" for a cluster with a mass of $10^{15}\ M_\odot$ at the present time (Randall & Sarazin 2001). At least to the extent that the development of a cluster can be treated as a series of separate, discrete merger events separated by periods of approximate equilibrium (the "punctuated equilibrium" model; Cavaliere, Menci, & Tozzi 1999), these merger histories can be used to determine the effects of mergers on clusters.

2.2. ESTIMATES OF MERGER KINEMATICS

I now give some simple analytic argments to estimate the kinematics of an individual binary merger collision. The kinematic quantities describing the merger are defined in Figure 1.2, which is taken from Ricker & Sarazin (2001). The two subclusters have masses M_1 and M_2. Let d be the separation of the centers of the two subclusters, let v be the relative velocity of the centers, and let b be the impact parameter of the collision.

2.2.1 Turn-Around Distances. Assume that the two subclusters of mass M_1 and M_2 merge at some time $t_{\rm merge}$ (the age of the Universe at the time of the merger). It is assumed that the two subclusters have fallen together from a large distance d_0 with (possibly)

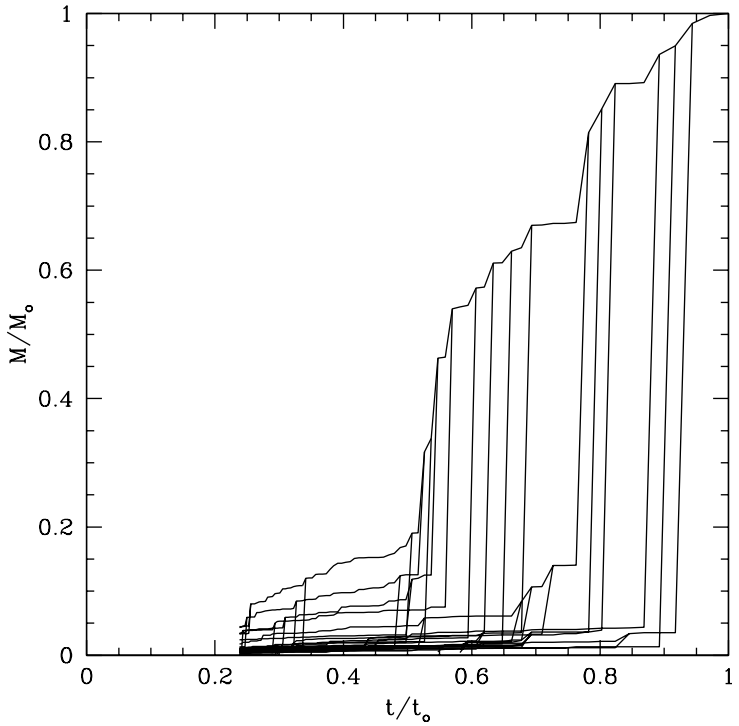

Figure 1.1. An example of a PS merger tree for a cluster of galaxies with a final mass of $M_0 = 10^{15} h^{-1}\, M_\odot$ (Randall & Sarazin 2001). The mass is shown as a function of the age of the Universe t; the present age is t_0. This model was for an open Universe with $\Omega_0 = 0.3$ and $\Omega_\Lambda = 0$.

nonzero angular momentum. (The exact value of d_0 does not affect the collision velocity very strongly as long as it is large and the infall velocity approaches free-fall from infinity.) For the purpose of computing the initial relative velocity, we approximate the two clusters as point masses. We assume that the two subclusters were initially expanding away from one another in the Hubble flow, and that their radial velocity was zero at their greatest separation d_0. If we assume that the two subclusters dominate the mass in the region of the Universe they occupy, we can treat their initial expansion and recollapse as the orbit of two point masses, and Kepler's Third Law gives the greatest separation as

$$\begin{aligned} d_0 &\approx [2G\,(M_1 + M_2)]^{1/3} \left(\frac{t_{\rm merge}}{\pi}\right)^{2/3} \\ &\approx 4.5 \left(\frac{M_1 + M_2}{10^{15}\, M_\odot}\right)^{1/3} \left(\frac{t_{\rm merge}}{10^{10}\,{\rm yr}}\right)^{2/3} {\rm Mpc}\,. \end{aligned} \tag{10}$$

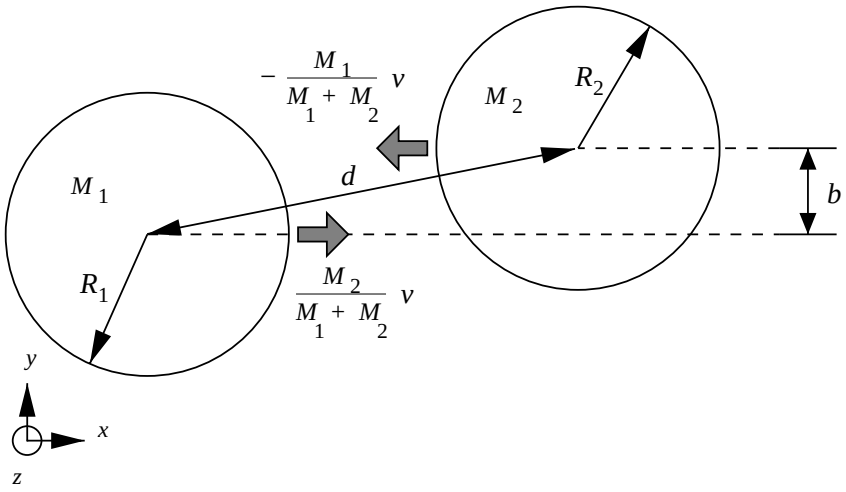

Figure 1.2. A schematic diagram of the kinematics for a merger between two subclusters of masses M_1 and M_2 and radii R_1 and R_2. The separation of the cluster centers is d, and the impact parameter is b, and the initial relative velocity is v.

2.2.2 Merger Velocities. At the separation d_0, the clusters are assumed to have zero relative radial velocity; hence their orbital angular momentum and energy are

$$\begin{aligned} J_{\rm orb} &\approx mv_0d_0 \\ E_{\rm orb} &\approx \frac{1}{2}mv_0^2 - \frac{GM_1M_2}{d_0} \ , \end{aligned} \tag{11}$$

where their reduced mass is

$$m \equiv \frac{M_1M_2}{M_1+M_2} \ , \tag{12}$$

and v_0 is their initial relative transverse velocity. At the separation d, the relative velocity v is perpendicular to the direction of b, so we can write

$$\begin{aligned} J_{\rm orb} &\approx mvb \\ E_{\rm orb} &\approx \frac{1}{2}mv^2 - \frac{GM_1M_2}{d} \ . \end{aligned} \tag{13}$$

Conserving angular momentum and energy, we eliminate v_0 and find

$$v^2 \approx 2G\left(M_1+M_2\right)\left(\frac{1}{d}-\frac{1}{d_0}\right)\left[1-\left(\frac{b}{d_0}\right)^2\right]^{-1} \ , \tag{14}$$

or

$$v \approx 2930 \left(\frac{M_1 + M_2}{10^{15}\, M_\odot}\right)^{1/2} \left(\frac{d}{1\,\mathrm{Mpc}}\right)^{-1/2} \left[\frac{1 - \frac{d}{d_0}}{1 - \left(\frac{b}{d_0}\right)^2}\right]^{1/2} \mathrm{km\,s^{-1}}\,. \quad (15)$$

2.2.3 Angular Momenta, Impact Parameters, and Transverse Velocities. The remaining kinematic parameter for the merger is the impact parameter b, or equivalently the orbital angular momentum J_{orb} or the initial tangential velocity v_0. In principal, a range of values are possible for mergers of subclusters with similar masses and similar merger epochs t_{merge}. The angular momentum will be determined by tidal torques from surrounding material. Thus, I give a estimate of the range of possible values based on the linear-theory result for the dimensionless spin of dark-matter halos; this argument is given in Ricker & Sarazin (2001). The spin parameter λ is defined as (Peebles 1969)

$$\lambda \equiv \frac{J|E|^{1/2}}{GM^{5/2}}\,. \quad (16)$$

Here J is the total angular momentum of the halo, E is its total energy, and M is its mass. In linear theory, the average value of λ is expected to be approximately constant, independent of the mass of the halo. Recently, Sugerman, Summers, and Kamionkowski (2000) have performed a detailed comparison of linear-theory predictions to actual angular momenta of galaxies formed in cosmological N-body/hydro calculations. These simulations did not include cooling or star formation, so at the upper end of the mass range they studied their results should carry over to clusters. They find, in agreement with White (1984), that linear theory overpredicts the final angular momentum of galaxies by roughly a factor of three, with a large ($\sim 50\%$) dispersion in the ratio of the linear-theory prediction to the actual value. However, given the uncertainties, the angular momenta agree with the results in equation (16) for a value of $\lambda \approx 0.05$. Thus, we will assume that the average total angular momenta of clusters of galaxies are given by

$$J \approx \frac{\lambda G M^{5/2}}{|E|^{1/2}}\,, \quad (17)$$

with $\lambda \approx 0.05$. The normal virial relations for clusters imply that the energies of clusters scale with their mass as $|E| \propto M^{5/3}$, which implies that the angular momenta scale as $J \propto M^{5/3}$ as well.

Let us take the halo to be the final merged cluster. Its final total angular momentum is the sum of the angular momenta of the two subclusters plus the orbital angular momentum $J_{\rm orb}$. Applying equation (17) to the initial masses M_1 and M_2 and the final mass $M_1 + M_2$ and taking the difference gives the orbital angular momentum $J_{\rm orb}$. We assume that the angular momenta are correlated (i.e., that they lie along the same direction), since they are all produced by approximately the same local tidal field. The final energy of the merged cluster is the sum of the energies of the initial subclusters plus the orbital energy $E_{\rm orb}$. The rotational kinetic energies can be ignored as they are only a fraction $\sim 2\lambda^2 \lesssim 1\%$ of the total energies.

Using these relations, the average orbital angular momentum of the merger is found to be

$$J_{\rm orb} \approx \frac{\lambda G M_1 M_2}{\left[\frac{G(M_1+M_2)}{d_0} - \frac{1}{2}v_0^2\right]^{1/2}} f(M_1, M_2)\,. \tag{18}$$

Here, the function $f(M_1, M_2)$ corrects for the internal angular momenta and energy of the subclusters. This correction can be written as

$$f(M_1, M_2) \equiv \frac{(M_1+M_2)^3}{M_1^{3/2} M_2^{3/2}} \left[1 - \frac{\left(M_1^{5/3} + M_2^{5/3}\right)}{(M_1+M_2)^{5/3}}\right]^{3/2}\,, \tag{19}$$

but it only depends on the ratio $(M_</M_>)$ of the smaller to larger mass of the two subclusters. It varies between $4(2^{2/3}-1)^{3/2} \approx 1.80 \leq f(M_1, M_2) \leq (5/3)^{3/2} \approx 2.15$, so that $f(M_1, M_2) \approx 2$. The kinetic energy term $v_0^2/2$ in the denominator of equation (18) can be shown to be approximately $2\lambda^2 \approx 1\%$ of the potential energy term. Thus, this term can be dropped to yield

$$J_{\rm orb} \approx \lambda M_1 M_2 \sqrt{\frac{G d_0}{M_1+M_2}}\, f(M_1, M_2)\,. \tag{20}$$

The corresponding initial transverse velocity is

$$\begin{aligned} v_0 &\approx \lambda \sqrt{\frac{G(M_1+M_2)}{d_0}}\, f(M_1, M_2) \\ &\approx 93 \left(\frac{\lambda}{0.05}\right) \left(\frac{M_1+M_2}{10^{15}\,M_\odot}\right)^{1/2} \left(\frac{d_0}{5\,{\rm Mpc}}\right)^{-1/2} \left(\frac{f}{2}\right) {\rm km\,s^{-1}}\,. \end{aligned} \tag{21}$$

After the clusters have fallen towards one another to a separation d, the impact parameter for the collision is (Figure 1.2)

$$b \approx \left(\frac{v_0}{v}\right) d_0\,, \tag{22}$$

where the infall velocity is given by equation (15). Note that equation (22) implies that $b \ll d_o$, so that one can drop the (b/d_0) term in equation (15). Substituting equations (15) & (21) into equation (22) gives

$$\begin{aligned} b &\approx \lambda \sqrt{\tfrac{d_0 d}{2}} \left(1 - \tfrac{d}{d_0}\right)^{-1/2} f(M_1, M_2) \\ &\approx 160 \left(\tfrac{\lambda}{0.05}\right) \left(\tfrac{d}{1\,\mathrm{Mpc}}\right)^{1/2} \left(\tfrac{d_0}{5\,\mathrm{Mpc}}\right)^{1/2} \left(1 - \tfrac{d}{d_0}\right)^{-1/2} \left(\tfrac{f}{2}\right) \mathrm{kpc}\,. \quad (23) \end{aligned}$$

Thus, most mergers are expected to involve fairly small impact parameters, comparable to the sizes of the gas cores in clusters. Many examples are known of mergers where the X-ray morphology suggests a small offset; an example is the merger in the cluster surrounding Cygnus-A (Markevitch, Sarazin, & Vikhlinin 1999). However, the preceding arguments are approximate and statistical, and mergers with larger impact parameters are also expected to occur; based on the X-ray image and temperature map, it is likely that Abell 3395 is an example of such a merger (Markevitch et al. 1998). Larger impact parameters may occur in mergers involving more than two subclusters. On the other hand, the distribution of impact parameters may be biased to lower values if most mergers occur along large scale structure filaments (e.g., Evrard & Gioia 2001).

3. THERMAL PHYSICS OF MERGER SHOCKS

The intracluster medium (ICM) is generally close to hydrostatic equilibrium in clusters which are not undergoing strong mergers. The virial theorem then implies that the square of the thermal velocity (sound speed) of the ICM is comparable to the gravitational potential. During a merger, the infall velocities of the subclusters (equation 15) are comparable to the escape velocity, which implies that the square of the infall velocity is larger (by roughly a factor of two) than the gravitational potential. Thus, the motions in cluster mergers are expected to be supersonic, but only moderately so. As a result, one expects that cluster mergers will drive shock waves into the intracluster gas of the two subclusters. Let v_s be the velocity of such a shock wave relative to the preshock intracluster gas. The sound speed in the preshock gas is $c_s = \sqrt{(5/3)P/\rho}$, where P is the gas pressure and ρ is the density. Then, the Mach number of the shock is $\mathcal{M} \equiv v_s/c_s$. Based on the simple argument given above and confirmed by merger simulations (Schindler & Müller 1993; Roettiger, Stone, & Burns 1999; Ricker & Sarazin 2001; Schindler 2001), one expects shocks with Mach numbers of $\mathcal{M} \lesssim 3$.

Stronger shocks may occur under some circumstances, such as in the outer parts of clusters, or in low mass subclusters merging with more massive clusters. However, in the latter case, the shocks in the less massive subcluster may also be weak if the intergalactic gas in the smaller subcluster is denser than that in the more massive subclusters (§ 4).

Shocks are irreversible changes to the gas in clusters, and thus increase the entropy S in the gas. A useful quantity to consider is the specific entropy per particle in the gas, $s \equiv S/N$, where N is the total number of particles. To within additive constants, the specific entropy of an ideal gas is

$$\begin{aligned} s &= \frac{3}{2}\, k\, \ln\left(\frac{P}{\rho^{5/3}}\right) , \\ &= \frac{3}{2}\, k\, \ln\left(\frac{T}{\rho^{2/3}}\right) , \end{aligned} \tag{24}$$

where T is the gas temperature. Observations of X-ray spectra can be used to determine T, while the X-ray surface brightness depends on ρ^2. Thus, one can use X-ray observations to determine the specific entropy in the gas just before and just after apparent merger shocks seen in the X-ray images. Since merger shocks should produce compression, heating, pressure increases, and entropy increases, the corresponding increase in all of these quantities (particularly the entropy) can be used to check that discontinuities are really shocks (e.g., not "cold fronts" or other contact discontinuities, § 4.2).

Markevitch et al. (1999) applied this test to ASCA temperature maps and ROSAT images of Cygnus-A and Abell 3667, two clusters which appeared to show strong merger shocks. (Recent Chandra images have cast doubt on the interpretation of Abell 3667 [Vikhlinin, Markevitch, & Murray 2001b].) In Cygnus-A, the increase in specific entropy in the shocked regions is roughly $\Delta s \approx (3/2)k$. The specific heat per particle q which must be dissipated to produce this change in entropy is $q \approx T\Delta s \approx (3/2)kT$, or about the present specific heat content in the shocked gas. Thus, these observations provide a direct confirmation that merger shocks contribute significantly to the heating of the intracluster gas.

3.1. SHOCK KINEMATICS

The variation in the hydrodynamical variables in the intracluster medium across a merger shock are determined by the standard Rankine–Hugoniot jump conditions (e.g., Landau & Lifshitz 1959, § 85), if one assumes that all of the dissipated shock energy is thermalized. Consider a small element of the surface of a shock (much smaller than the radius

of curvature of the shock, for example). The tangential component of the velocity is continuous at the shock, so it is useful to go to a frame which is moving with that element of the shock surface, and which has a tangential velocity which is equal to that of the gas on either side of the shock. In this frame, the element of the shock surface is stationary, and the gas has no tangential motion. Let the subscripts 1 and 2 denote the preshock and postshock gas; thus, $v_1 = v_s$ is the longitudinal velocity of material into the shock (or alternative, the speed with which the shock is advancing into the preshock gas). Conservation of mass, momentum, and energy then implies the following jump conditions

$$\begin{aligned} \rho_1 v_1 &= \rho_2 v_2 \,, \\ P_1 + \rho_1 v_1^2 &= P_2 + \rho_2 v_2^2 \,, \\ w_1 + \frac{1}{2} v_1^2 &= w_2 + \frac{1}{2} v_2^2 \,. \end{aligned} \tag{25}$$

Here, $w = P/\rho + \epsilon$ is the enthalpy per unit mass in the gas, and ϵ is the internal energy per unit mass. If the gas behaves as a perfect fluid on each side of the shock, the internal energy per unit mass is given by

$$\epsilon = \frac{1}{\gamma_{\rm ad} - 1} \frac{P}{\rho} \,, \tag{26}$$

where $\gamma_{\rm ad}$ is the ratio of specific heats (the adiabatic index) and is $\gamma_{\rm ad} = 5/3$ for fully ionized plasma. The jump conditions can be rewritten as:

$$\begin{aligned} \frac{P_2}{P_1} &= \frac{2\gamma_{\rm ad}}{\gamma_{\rm ad}+1} \mathcal{M}^2 - \frac{\gamma_{\rm ad}-1}{\gamma_{\rm ad}+1} \\ \frac{v_2}{v_1} = \frac{\rho_1}{\rho_2} \equiv \frac{1}{C} &= \frac{2}{\gamma_{\rm ad}+1} \frac{1}{\mathcal{M}^2} + \frac{\gamma_{\rm ad}-1}{\gamma_{\rm ad}+1} \,, \end{aligned} \tag{27}$$

where $C \equiv \rho_2/\rho_1$ is the shock compression.

If one knew the velocity structure of the gas in a merging cluster, one could use these jump condition to derive the temperature, pressure, and density jumps in the gas. At present, the best X-ray spectra for extended regions in clusters of galaxies have come from CCD detectors on ASCA, Chandra, and XMM/Newton. CCDs have a spectral resolution of >100 eV at the Fe K line at 7 keV, which translates into a velocity resolution of >4000 km/s. Thus, this resolution is (at best) marginally insufficient to measure merger gas velocities in clusters. In a few cases with very bright regions and simple geometries, the grating spectrometers on Chandra and especially XMM/Newton may be useful. However, it is likely that the direct determinations of gas velocities in most clusters will wait for the launch of higher spectral resolution nondispersive spectrometers on Astro-E2 and Constellation-X.

At present, X-ray observations can be used to directly measure the temperature and density jumps in merger shocks. Thus, one needs to invert the jump relations to give the merger shock velocities for a given shock temperature, pressure, and/or density increase. If the temperatures on either side of the merger shock can be measured from X-ray spectra, the shock velocity can be inferred from (Markevitch, Sarazin, & Vikhlinin 1999)

$$\Delta v_s = \left[\frac{kT_1}{\mu m_p}\,(C-1)\left(\frac{T_2}{T_1}-\frac{1}{C}\right)\right]^{1/2}\,, \tag{28}$$

where $\Delta v_s = v_1 - v_2 = [(C-1)/C]v_s$ is the velocity change across the shock, and μ is the mean mass per particle in units of the proton mass m_p. The shock compression C can be derived from the temperatures as

$$\frac{1}{C} = \left[\frac{1}{4}\left(\frac{\gamma_{\rm ad}+1}{\gamma_{\rm ad}-1}\right)^2\left(\frac{T_2}{T_1}-1\right)^2 + \frac{T_2}{T_1}\right]^{1/2} - \frac{1}{2}\frac{\gamma_{\rm ad}+1}{\gamma_{\rm ad}-1}\left(\frac{T_2}{T_1}-1\right)\,. \tag{29}$$

Alternatively, the shock compression can be measured directly from the X-ray image. However, it is difficult to use measurements of the shock compression alone to determine the shock velocity, for two reasons. First, a temperature is needed to set the overall scale of the velocities; as is obvious from equation (27), the shock compression allows one to determine the Mach number $\mathcal{M}$ but not the shock velocity. The second problem is that temperature or pressure information is needed to know that a discontinuity in the gas density is a shock, and not a contact interface (e.g., the "cold fronts" discussed in § 4.2 below).

X-ray temperature maps of clusters have been used to derive the merger velocities using these relations. Markevitch et al. (1999) used ASCA observations to determine the kinematics of mergers in three clusters (Cygnus-A, Abell 2065, and Abell 3667). Because of the poor angular resolution of ASCA, these analyses were quite uncertain. More recently, possible shocks have been detected in Chandra images of a number of merging clusters (e.g., Abell 85, Kempner, Sarazin, & Ricker 2001; Abell 665, Markevitch et al. 2001; Abell 3667, Vikhlinin et al. 2001b), and the shock jump conditions have been applied to determine the kinematics in these clusters.

The simplest case is a head-on symmetric merger ($b = 0$ and $M_1 = M_2$) at an early stage when the shocked region lies between the two cluster centers. Markevitch et al. (1999) suggest that the Cygnus-A cluster is an example. If the gas within the shocked region is nearly stationary, then the merger velocity of the two subclusters is just $v = 2\Delta v_s$. Applying these techniques to the ASCA temperature map for

the Cygnus-A cluster, Markevitch et al. found a merger velocity of $v \approx$ 2200 km/s. This simple argument is in reasonable agreement with the results of numerical simulations of this merger (Ricker & Sarazin 2001). The radial velocity distribution of the galaxies in this cluster is bimodal (Owen et al. 1997), and consistent with a merger velocity of ∼2400 km/s.

One can compare the merger velocities derived from the temperature jumps in the merger shocks with the values predicted by free-fall from the turn-around radius (equation 15). In the case of Cygnus-A, Markevitch et al. (1999) found good agreement with the the free-fall velocity of ∼2200 km/s. This consistency suggests that the shock energy is effectively thermalized, and that a major fraction does not go into turbulence, magnetic fields, or cosmic rays. Thus, the temperature jumps in merger shocks can provide an important test of the relative roles of thermal and nonthermal processes in clusters of galaxies. Further tests should be possible by comparing shock heating with velocities determined from optical redshifts, from direct velocity measurements in the gas with Astro-E2 and Constellation-X, and from infall arguments.

3.2. NONEQUILIBRIUM EFFECTS

Cluster mergers are expected to produce collisionless shocks, as occurs in supernova remnants. As such, nonequilibrium effects are expected, including nonequipartition of electrons and ions and nonequilibrium ionization (Markevitch et al. 1999; Takizawa 1999,2000). Collisionless shocks are generally not as effective in heating electrons as ions. Assuming that the postshock electrons are somewhat cooler than the ions, the time scale for electron and protons to approach equipartition as a result of Coulomb collisions in a hot ionized gas is (Spitzer 1962)

$$\begin{aligned} t_{\rm eq} &= \frac{3 m_p m_e}{8\sqrt{2\pi} n_e e^4 \ln\Lambda} \left(\frac{k T_e}{m_e}\right)^{3/2} \\ &\approx 2.1 \times 10^8 \left(\frac{T_e}{10^8\,{\rm K}}\right)^{3/2} \left(\frac{n_e}{0.001\,{\rm cm}^{-3}}\right)^{-1} {\rm yr}\,, \end{aligned} \tag{30}$$

where n_e and T_e are the electron number density and temperature, respectively, and Λ is the Coulomb factor. The relative velocity between the postshock gas and the shock front is $(1/4)v_s$; thus, one would expect the electron temperature to reach equipartition a distance of

$$d_{\rm eq} \approx 160 \left(\frac{v_s}{3000\,{\rm km/s}}\right) \left(\frac{T_e}{10^8\,{\rm K}}\right)^{3/2} \left(\frac{n_e}{0.001\,{\rm cm}^{-3}}\right)^{-1} {\rm kpc} \tag{31}$$

behind the shock front. Of course, it is the electron temperature (rather than the ion or average temperature) which determines the shape of the

X-ray spectrum. This distance is large enough to insure that the lag could be spatially resolved in X-ray observations of low redshift clusters. Similar effects might be expected through non-equilibrium ionization.

On the other hand, it is likely that the nonequilibrium effects in cluster merger shocks are much smaller than those in supernova blast wave shocks because of the low Mach numbers of merger shocks. That is, the preshock gas is already quite hot (both electrons and ions) and highly ionized. Moreover, a significant part of the heating in low Mach number shocks is due to adiabatic compression, and this would still act on the electrons in the postshock gas in merger shocks, even if there were no collisionless heating of electrons. For example, in a $\mathcal{M} = 2$, $\gamma_{\rm ad} = 5/3$ shock, the total shock increase in temperature is a factor of 2.08 (eq. 27). The shock compression is $C = 2.29$, so adiabatic compression increases the electron temperature by a factor of $C^{2/3} = 1.74$, which is about 83% of the shock heating.

4. MERGERS AND COOL CLUSTER CORES

4.1. COOLING FLOWS VS. MERGERS

The centers of a significant fraction of clusters of galaxies have luminous cusps in their X-ray surface brightness known as "cooling flows" (see Fabian 1994 for an extensive review). In every case, there is a bright (cD) galaxy at the center of the cooling flow region. The intracluster gas densities in these regions are much higher than the average values in the outer portions of clusters. X-ray spectra indicate that there are large amounts of gas at low temperatures (down to $\sim 10^7$ K), which are much cooler than those in the outer parts of clusters. The high densities imply rather short cooling times $t_{\rm cool}$ (the time scale for the gas to cool to low temperature due to its own radiation). The hypothesis is that the gas in these regions is cooling from higher intracluster temperature ($\sim 10^8$ K) down to these lower temperatures as a result of the energy loss due to the X-ray emission we observe. Typical cooling rates are ~ 100 $M_\odot$ yr^{-1}. The cooling times, although much shorter than the Hubble time, are generally much longer than the dynamical (i.e., sound crossing time) of the gas in these regions. As a result, the gas is believed to remain nearly in hydrostatic equilibrium. Thus, the gas must compress as it cools to maintain a pressure which can support the weight of the overlying intracluster medium.

The primary observational characteristics of cooling flows are very bright X-ray surface brightnesses which increase rapidly toward the center of the cluster. The high surface brightnesses imply high gas densities

which also increase rapidly towards the cluster center. These regions contain cooler cluster gas.

Empirically, there is significant indirect evidence that mergers disrupt cooling flows. There is a strong statistical anticorrelation between cooling flows and/or cooling rates, and irregular structures in clusters as derived by statistical analysis of their X-ray images (Buote & Tsai 1996). The irregular structures are often an indication of an ongoing merger. Looked at individually, very large cooling flows are almost never associated with very irregular or bimodal clusters, which are likely merger candidates (Henriksen 1988; Edge, Stewart, & Fabian 1992). There are some cases of moderate cooling flows in merging clusters; in most cases, these appear to be early-stage mergers where the merger shocks haven't yet reached the cooling core of the cluster. Examples may include Cygnus-A (Arnaud et al. 1984; Owen et al. 1997; Markevitch et al. 1999) and Abell 85 (Kempner et al. 2001). There also are a large number of merging clusters at a more advanced stage with relatively small cooling cores, both in terms of the cooling rate and the physical radius; Abell 2065 (Markevitch et al. 1999) may be an example. Recently, Chandra Observatory X-ray images have shown a number of merging clusters with rapidly moving cores of cool gas (the "cold fronts" discussed below in § 4.2). In these systems, the cooling flows appear to have survived, at least to the present epoch in the merger.

It is unclear exactly how and under what circumstances mergers disrupt cooling flows. The cooling flows might be disrupted by tidal effects, by shock heating the cooler gas, by removing it dynamically from the center of the cluster due to ram pressure, by mixing it with hotter intracluster gas, or by some other mechanism. Numerical hydrodynamical simulations are needed to study the mechanisms by which cooling flows are disrupted. This is a relatively unexplored area, largely because the small spatial scales and rapid cooling time scales in the inner regions of cooling flows are still a significant challenge to the numerical resolution of hydrodynamical codes. McGlynn & Fabian (1984) argued that mergers disrupted cooling flows, but this was based on purely N-body simulations. Recently, Gòmez et al. (2001) have made hydrodynamical simulations of the effects of head-on mergers with relatively small subclusters (1/4 or 1/16 of the mass of the main cluster) on a cooling flow in the main cluster. They find that the mergers disrupt the cooling flow in some cases, but not in others. Their simulations suggest that the disruption is not due to tidal or other gravitational effects.

Another possibility is that the merger shocks heat up the cooling flow gas and stop the cooling flow. In the simulations, this does not appear to be the main mechanism of cooling flow disruption. There are

a number of simple arguments which suggest that merger shocks should be relatively inefficient at disrupting cooling flows. First, it is difficult for these shocks to penetrate the high densities and steep density gradients associated with cooling flows, and the merger shocks would be expected to weaken as they climb these steep density gradients. Even without this weakening, merger shocks have low Mach numbers, and only produce rather modest increases in temperature ($\lesssim$ a factor of 2). These small temperature increases are accompanied by significant compressions. As a result, shock heating actually decreases the cooling time due to thermal bremsstrahlung emission for shocks with Mach numbers $\mathcal{M} \leq (21 + 12\sqrt{3})^{1/2} \approx 6.5$. It is likely that the shocked gas will eventually expand, and adiabatic expansion will lengthen the cooling time. However, even if the gas expands to its preshock pressure, the increase in the cooling time is not very large. For a $\mathcal{M} = 2$ shock, the final cooling time after adiabatic expansion to the original pressure is only about 18% longer than the initial cooling time.

The simulations by Gòmez et al. suggest that the main mechanism for disrupting cooling flows is associated with the ram pressure of gas from the merging subcluster. The gas in the cooling flow is displaced, and may eventually mix with the hotter gas (see also Ricker & Sarazin 2001). Earlier, Fabian & Daines (1991) had argued that ram pressure, rather than shock heating, was the main mechanism for disrupting cooling flows. Assuming this is the case, one expects that the merger will remove the cooling flow gas at radii which satisfy

$$\rho_{\rm sc} v_{\rm rel}^2 \gtrsim P_{\rm CF}(r)\,, \tag{32}$$

where $P_{\rm CF}(r)$ is the pressure profile in the cooling flow, $\rho_{\rm sc}$ is the density of the merging subcluster gas at the location of the cooling flow, and $v_{\rm rel}$ is the relative velocity of the merging subcluster gas and the cooling flow. Gòmez et al. (2001) find that this relation provides a reasonable approximation to the disruption in their simulations.

The pressure profile in the cooling flow gas prior to the merger is determined by the condition of hydrostatic equilibrium. If the cluster gravitational potential has a wide core within which the potential is nearly constant (e.g., as in a King model), then the cooling flow pressure will not increase rapidly into the center. In this case, once the merger reaches the central regions of the cluster, if the ram pressure is sufficient to remove the outer parts of the cooling flow, it should be sufficient to remove nearly all of the cooling flow. On the other hand, if the cluster potential is sharply peaked (as in a NFW profile, Navarro, Frenk, & White 1997), the merger may remove the outer parts of the cooling flow but not the innermost regions. Thus, the survival and size of

cool cores in merging clusters can provide evidence on whether clusters have sharply peaked potentials. Markevitch et al. (1999) applied this argument to the two small cool cores in the merging cluster Abell 2065, and concluded that steep central potentials, consistent with the NFW model, were needed.

4.2. COLD FRONTS

One of the more dramatic early discoveries with the Chandra X-ray Observatory was the presence of very sharp surface brightness discontinuities in merging clusters of galaxies (e.g., Forman 2001). A pair of such discontinuities were first seen in the public science verification data on the Abell 2142 cluster (Markevitch et al. 2000). Initially, it seemed likely that these were merger shocks. However, temperature measurements showed that this was not the case. The high X-ray surface brightness regions were both dense and *cool*; thus, the gas in these regions had a lower specific entropy than the gas in the less dense regions. Shocks are irreversible processes which must increase the entropy as the gas is compressed. Also, the gas pressure appeared to be continuous across the density discontinuity. The lack of a pressure jump and the incorrect sign of the temperature and entropy variations showed that these features could not be shocks (Markevitch et al. 2000).

Instead, they appear to be contact discontinuities between hot, diffuse gas and a cloud of colder, denser gas (Markevitch et al. 2000). The cold cloud is moving rapidly through the hotter gas; Vikhlinin et al. (2001b) refer to this situation as a "cold front." The cold cloud is being distorted and, presumably, stripped by the hot gas, but has survived to the epoch of the observation. Markevitch et al. (2000) argue that the source of the cold cloud is the core of one of the merging subclusters; in Abell 2142, both of the subcluster cores appear to have survived. There are several reasons why the core gas is much denser than the surrounding hot gas. First, prior to mergers, clusters are generally stably-stratified, with the denser, lower entropy gas at the center. Thus, the core density will be much higher than the density of the outer gas in a cluster. Second, in hierarchical large scale structure, smaller subclusters generally form from denser perturbations, so small merging subclusters may have cores with quite high densities. Third, many rich and poor clusters have cooling flows at their centers (§ 4.1), and these regions have very high densities and relatively low temperatures. As noted above, cooling flows do appear to be able to partially survive in mergers, at least for some period.

Subsequently, cold fronts have been observed in a number of other clusters, including Abell 3667 (Vikhlinin et al. 2001b), RXJ1720.1+2638

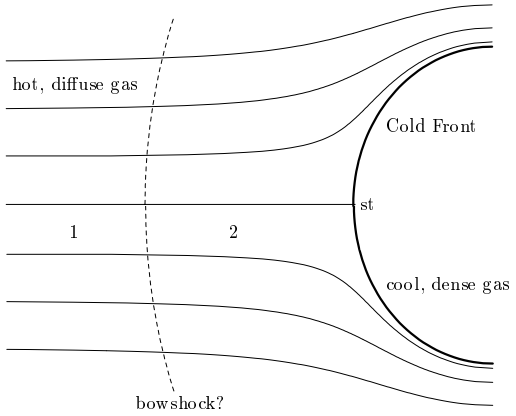

Figure 1.3. A schematic diagram of flow around a "cold front" in a cluster merger. The heavy solid arc at the right represents the contact discontinuity between the cold, dense cold core gas, and the hotter, more diffuse gas from the outer regions of the other cluster. The cold core is moving toward the left relative to the hotter gas. The narrow solid lines are streamlines of the flow of the hotter gas around the cold core. The region labelled "1" represent the upstream, undisturbed hot gas. If the cold front is moving transonically ($\mathcal{M}_1 > 1$), then the cold front will be preceded by a bow shock, which is shown as a dashed arc. The stagnation point, where the relative velocity of the cooler dense gas and hotter diffuse gas is zero, is marked "st".

(Mazzotta et al. 2001), Abell 85 (Kempner et al. 2001), and possibly Abell 754 and Abell 2163 (Markevitch et al. 2001). The most detailed analysis has been made for Abell 3667, and my discussion closely follows the arguments given in Vikhlinin et al. (2001b).

4.2.1 Kinematics of Cold Fronts. As discussed extensively in Vikhlinin et al. (2001b), the variation in the density, pressure, and temperature of the gas in a cold front can be used to determine the relative velocity of cold core. This technique is analogous to that for merger shocks discussed above (eqs. 28 & 29). The geometry is illustrated in Figure 1.3, which is drawn in the rest frame of the cold core. We assume that the cold core has a smoothly curved, blunt front edge. The normal component of the flow of hot gas past the surface of the cold core will be zero. There will be at least one point where the flow is perpendicular to the surface of the cold core, and the flow velocity of the hot gas will be zero at this stagnation point ("st" in Fig. 1.3). Far upstream, the flow of the hot gas will be undisturbed at the velocity of the cold core relative to the hotter gas, v_1. Let c_{s1} be the sound speed in this upstream gas, and $\mathcal{M}_1 \equiv v_1/c_{s1}$ be the Mach number of the motion of the cold core

into the upstream gas. If $\mathcal{M}_1 > 1$, a bow shock will be located ahead of the cold front.

The ratio of the pressure at the stagnation point to that far upstream is given by (e.g., Landau & Lifshitz 1959, § 114).

$$\frac{P_{\rm st}}{P_1} = \begin{cases} \left(1 + \frac{\gamma_{\rm ad}-1}{2}\mathcal{M}_1^2\right)^{\frac{\gamma_{\rm ad}}{\gamma_{\rm ad}-1}}, & \mathcal{M}_1 \leq 1\,, \\ \mathcal{M}_1^2 \left(\frac{\gamma_{\rm ad}+1}{2}\right)^{\frac{\gamma_{\rm ad}+1}{\gamma_{\rm ad}-1}} \left(\gamma_{\rm ad} - \frac{\gamma_{\rm ad}-1}{2\mathcal{M}_1^2}\right)^{-\frac{1}{\gamma_{\rm ad}-1}}, & \mathcal{M}_1 > 1\,. \end{cases} \tag{33}$$

The ratio $(P_{\rm st}/P_1)$ increases continuously and monotonically with $\mathcal{M}_1$. Thus, in principle, measurements of P_1 and $P_{\rm st}$ in the hot gas could be used to determine $\mathcal{M}_1$. The pressures would be determined from X-ray spectra and images. In practice, the emissivity of the hot gas near the stagnation point is likely to be small. However, the pressure is continuous across the cold front, so the stagnation pressure can be determined just inside of the cold core, where the X-ray emissivity is likely to be much higher. Once $\mathcal{M}_1$ has been determined, the velocity of the encounter is given by $v_1 = \mathcal{M}_1 c_{s1}$.

If the motion of the cold core is transonic ($\mathcal{M}_1 > 1$), one can also determine the velocity from the temperature and/or density jump at the bow shock (eqs. 28 & 29). If the bow shock can be traced to a large transverse distance and forms a cone, the opening angle of this Mach cone corresponds to the Mach angle, $\theta_M \equiv \csc^{-1}(\mathcal{M}_1)$. However, variations in the cluster gas temperature may lead to distortions in this shape.

The distance between the stagnation point and the closest point on the bow shock (the shock "stand-off" distance d_s) can also be used to estimate the Mach number of the motion of the cold front (Vikhlinin et al. 2001b). The ratio of d_s to the radius of curvature of the cold front $R_{\rm cf}$ depends on the Mach number $\mathcal{M}_1$ and on the shape of the cold front. Figure 1.4 shows the values of $d_s/R_{\rm cf}$ as a function of $(\mathcal{M}_1^2 - 1)^{-1}$ for a spherical cold front (Schreier 1982). Although there is no simple analytic expression for the stand-off distance which applies to all shapes of objects, a fairly general approximate method to calculate d_s has been given by Moekel (1949), and some simple approximate expressions exist for a number of simple geometries (Guy 1974; Radvogin 1974). The stand-off distance increases as the Mach number approaches unity; thus, this method is, in some ways, a very sensitive diagnostic for the Mach number for the low values expected in cluster mergers. On the other hand, the stand-off distance also depends strongly on the shape of the cold front as the Mach number decreases. The application of this diagnostic to observed clusters is strongly affected by projection effects. Because the radius of curvature of the bow shock is usually greater than

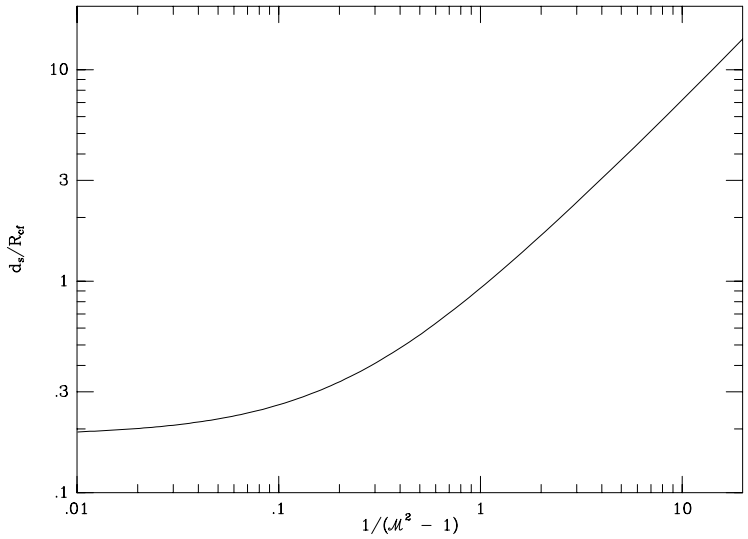

Figure 1.4. The ratio of the stand-off distance of the bow shock d_s to the radius of curvature $R_{\rm cf}$ of the stagnation region of the cold front, as a function of $1/(\mathcal{M}_1^2 - 1)$, where $\mathcal{M}_1$ is the Mach number. This is for a spherical cold front and $\gamma_{\rm ad} = 5/3$.

that of the cold front (Rusanov 1976), projection effects will generally cause d_s to be overestimated and $\mathcal{M}_1$ to be underestimated. Projection effects also make the true shape of the cold front uncertain.

These techniques have been used to determine the merger velocities from cold fronts in Abell 3667 (Vikhlinin et al. 2001b), RXJ1720.1+2638 (Mazzotta et al. 2001), and Abell 85 (Kempner et al. 2001).

4.2.2 Width of Cold Fronts. One remarkable aspect of the cold fronts observed with the Chandra Observatory in several clusters is their sharpness. In Abell 3667, the temperature changes by about a factor of two across the cold front (Vikhlinin et al. 2001b), and the accompanying change in the X-ray surface brightness occurs in a region which is narrower than 2 kpc (Vikhlinin et al. 2001b). This is less than the mean-free-path of electrons in this region. The existence of this very steep temperature gradient and similar results in other merging clusters with cold fronts requires that thermal conduction be suppressed by a large factor (Ettori & Fabian 2000; Vikhlinin, Markevitch, & Murray 2001a,b) relative to the classical value in an unmagnetized plasma (e.g., Spitzer 1962). It is likely that this suppression is due to the effects of the intracluster magnetic field. It is uncertain at this point whether this is due to a generally tangled magnetic field (in which case, heat conduction might be suppressed throughout clusters), or due to a tangential

magnetic field specific to the tangential flow at the cold front (Vikhlinin et al. 2001a).

Because of the tangential shear flow at the cold front (Fig. 1.3), the front should be disturbed and broadened by the Kelvin-Helmholtz (K-H) instability. Vikhlinin et al. (2001a) argue that the instability is suppressed by a tangential magnetic field, which is itself generated by the tangential flow. This suppression requires that the magnetic pressure P_B be a non-trivial fraction of the gas pressure P in this regions, $P_B \gtrsim 0.1P$. The required magnetic field strength in Abell 3667 is $B \sim 10$ μG.

5. NONTHERMAL PHYSICS OF MERGER SHOCKS

Cluster mergers involve shocks with velocities of $\sim$2000 km/s. Radio observations of supernova remnants indicate that shocks with these velocities can accelerate or reaccelerate relativistic electrons and ions (e.g., Blandford & Eichler 1987). In order to explain the general radio emission of supernova remnants, one requires that shocks in these systems generally convert a few percent of the shock energy into relativistic electrons. Even more energy may go into relativistic ions. Thus, one might expect that the intracluster medium would contain relativistic particles or cosmic rays, in addition to the hot thermal gas so evident in X-ray images. Given that all of the thermal energy content of the intracluster gas in clusters is due to shocks with velocities of $\gtrsim 10^3$ km/s, it seems likely that relativistic electrons and ions will have been accelerated with a total energy content of a few percent of the thermal energy in the hot gas. In massive, X-ray luminous clusters, the total thermal energy content in the ICM is $\gtrsim 3 \times 10^{63}$ ergs. Thus, merger or accretion shocks may have accelerated cosmic ray particles with a total energy content of $\gtrsim 10^{62}$ ergs. This would make clusters the largest individual sources of relativistic particles in the Universe; this energy probably exceeds that produced in active galactic nuclei, such as quasars and radio galaxies.

In a major merger, the thermal energy content of a cluster can be significantly increased by the merger shocks (§ 3). Thus, shock acceleration or reacceleration processes in a single merger may produce cosmic ray particles with a total energy of $\sim 10^{62}$ ergs. Thus, one would expect significant nonthermal effects associated with cluster mergers.

5.1. PARTICLE LIFETIMES AND LOSSES

Clusters are also very good storage locations for cosmic rays. These particles gyrate around magnetic field lines in the ICM. The magnetic field is frozen-in to the ionized thermal ICM, which is, in turn, bound

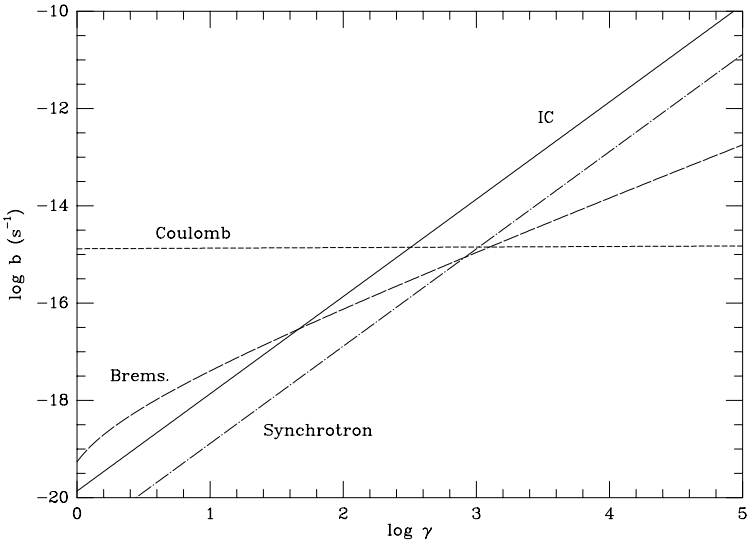

Figure 1.5. Values of the electron loss functions $b(\gamma)$ for inverse Compton (IC) emission, Coulomb losses, synchrotron emission, and bremsstrahlung emission as a function of $\gamma = E/(m_e c^2)$. The values assume $n_e = 10^{-3}$ cm^{-3}, $B = 1\,\mu$G, and redshift $z = 0$.

by the gravitational field of the cluster. Thus, the relativistic particles cannot simply stream out of a cluster. They can diffuse out along magnetic field lines. Diffusion is limited by scattering off of fluctuations in the magnetic field, and the rate is uncertain. However, under reasonable assumptions, the diffusion coefficient is approximately (Berezinsky, Blasi, & Ptuskin 1997; Colafrancesco & Blasi 1998)

$$D(E) \approx 2 \times 10^{29} \left(\frac{E}{1\,\mathrm{GeV}}\right)^{1/3} \left(\frac{B}{1\,\mu\mathrm{G}}\right)^{-1/3} \mathrm{cm}^2\,\mathrm{s}^{-1}\,, \qquad (34)$$

where E is the particle energy and B is the ICM magnetic field. The average time scale to diffuse out to a radius of R is about (Berezinsky et al. 1997; Colafrancesco & Blasi 1998)

$$t_{\mathrm{diff}} \approx \frac{R^2}{6D(E)} \approx 1 \times 10^{12} \left(\frac{R}{2\,\mathrm{Mpc}}\right)^2 \left(\frac{E}{1\,\mathrm{GeV}}\right)^{-1/3} \left(\frac{B}{1\,\mu\mathrm{G}}\right)^{1/3} \mathrm{yr}\,. \qquad (35)$$

Thus, under reasonable assumptions for the diffusion coefficient, particles with energies $\lesssim 10^6$ GeV have diffusion times which are longer than the Hubble time.

Relativistic particles can lose energy, and this can effectively remove them from the cosmic ray population. The time scales for energy loss by

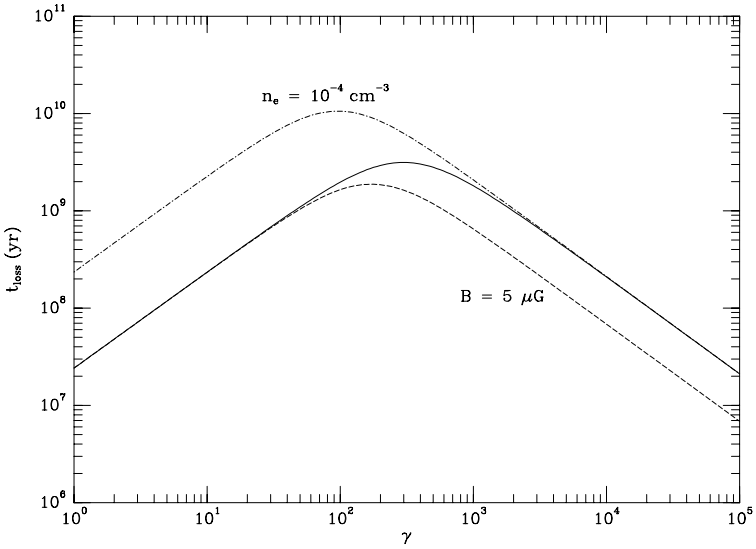

Figure 1.6. The solid curve gives the instantaneous loss time scale $t_{\rm loss}$ for relativistic electrons in a cluster with an electron density of $n_e = 10^{-3}$ cm^{-3} and a magnetic field of $B = 1$ μG. The short-dash curve is for $B = 5$ μG, while the dash-dot curve is for $n_e = 10^{-4}$ cm^{-3}.

ions are generally longer than the Hubble time. Electrons suffer losses due to interactions with ambient radiation fields (via inverse Compton [IC] emission), with the cluster magnetic field (via synchrotron emission), and with the intracluster gas (via Coulomb interactions and bremsstrahlung emission). However, the ICM is an extremely diffuse medium, and these losses are relatively small, at least as compared to the interstellar gas in our Galaxy. The gas density is low ($n_e \sim 10^{-3}$ cm^{-3}), reducing Coulomb and bremsstrahlung losses. The radiation fields are dilute, with the Cosmic Microwave Background (CMB) radiation providing the majority of the energy density. Magnetic fields are relatively weak; if the cluster fields are mainly smaller than 3 μG, then synchrotron losses are smaller than IC losses.

Let the energy of an electron be $E \equiv \gamma m_e c^2$, where γ is the Lorentz factor. Then, the energy loss of an electron can be written as

$$\frac{d\gamma}{dt} = \frac{1}{m_e c^2}\frac{dE}{dt} = -b(\gamma)\,, \tag{36}$$

assuming the loss is continuous. The values of the loss functions $b(\gamma)$ for various processes are shown in Figure 1.5 (Sarazin 1999a). It is clear that IC and synchrotron losses are dominant at high energies ($\gamma \gtrsim 200$ or

$E \gtrsim 100$ MeV), while Coulomb losses dominate at low energies ($\gamma \lesssim 200$ or $E \lesssim 100$ MeV).

One can define an instantaneous time scale for energy losses as $t_{\rm loss} \equiv \gamma/b(\gamma) = E/(dE/dt)$. Values for this loss time scale at the present epoch ($z = 0$) are shown in Figure 1.6 (Sarazin 1999a). The solid curve gives values assuming an average electron density of $n_e = 10^{-3}$ cm^{-3} and a magnetic field of $B = 1$ μG. For values of the magnetic field this small or lower, synchrotron losses are not very significant, and $t_{\rm loss}$ is nearly independent of B. The short dashed curve shows the effect of increasing the magnetic field to $B = 5$ μG; the losses at high energies are increased, and the loss time scales shortened. The dash–dot curve shows the loss time scale if the electron density is lowered to $n_e = 10^{-4}$ cm^{-3}. This reduces the losses at low energies, and increases the loss times there. Although high energy electrons lose energy rapidly due to IC and synchrotron emission, electrons with Lorentz factors of $\gamma \sim 300$ (energies ~ 150 MeV) have long lifetimes of $\sim 3 - 10$ Gyr, which are comparable to the likely ages of clusters (Sarazin & Lieu 1998; Sarazin 1999a). Thus, clusters of galaxies can retain low energy electrons ($\gamma \sim 300$) and nearly all cosmic ray ions for a significant fraction of a Hubble time.

5.2. SOURCES OF RELATIVISTIC PARTICLES

What are the sources for relativistic particles in clusters? One possibility is that these particles come from active galaxies (quasars, radio galaxies, etc.; e.g., Blasi & Colafrancesco 1999). Because luminous active galaxies were more common in the past, most of the cosmic ray particles would probably have been formed in the past. Another possibility is that these particles were generated as part of star formation in normal galaxies, either at the sites of star formation and supernova, or in galactic winds (e.g., Atoyan & Völk 2000). The galaxies in the inner regions of clusters today are mainly elliptical and S0 galaxies, which have old stellar populations. Thus, most of their star formation, and most of the particle production associated with it, probably occurred in the distant past. In any case, if AGNs or star bursts produced most of particles in clusters directly, then the cosmic ray populations in clusters would have no clear relation to mergers. I concentrate here on models in which the particles were either produced directly in mergers, or are the secondary products of particles produced in mergers, and/or were reaccelerated in mergers.

5.2.1 Particle Acceleration in Shocks. Radio observations of supernova remnants indicate that shocks with $v \gtrsim 10^3$ km/s convert at least a few percent of the shock energy into the acceleration of relativistic electrons (e.g., Blandford & Eichler 1987). Even more energy may go into relativistic ions. Thus, merger shocks seem like a natural acceleration site for relativistic particles. It is worth noting that there are significant differences between merger shocks and those associated with supernova blast waves. The merger shocks have relatively small Mach numbers, and as a result have smaller compressions. The ICM which enters the merger shock is hot. This means that the shocks are subsonic in the electrons; the preshock electrons have thermal velocities which are much greater than the shock velocities. On the other hand, the Alfvén Mach numbers ($\mathcal{M}_A \equiv v_s/v_A$ where $v_A = B^2/(4\pi\rho)$ is the Alfvén speed) for merger shocks can be quite large, $\mathcal{M}_A \gtrsim 30$. For some aspects of shock acceleration, the Alfvén Mach number is more relevant than the hydrodynamical Mach number.

Assuming that particles scatter repeatedly across the shock, these particles will undergo first-order Fermi shock acceleration. If the accelerating particles are treated as test particles, kinetic theory indicates that the particle spectrum is a power-law in the momentum p (Bell 1978; Blandford & Ostriker 1978):

$$N(p)\,dp = N_o \left(\frac{p}{mc}\right)^{-\mu} \frac{dp}{mc}\,, \qquad p_l \le p \le p_u \tag{37}$$

where m is the particle mass. Here, $N(p)\,dp$ is the number of particles with momenta between p and $p + dp$, and p_l (p_u) are the lower (upper) limits on the particle spectrum. If the particles are accelerated from nearly thermal energies, then the lower limit may be associated with the production of a nonthermal tail at the high energy end of the ICM thermal particle distribution. The upper limit may correspond to the highest energy for which acceleration is efficient (e.g., § 5.4.5). The particle spectrum expressed in terms of the Lorentz factor is

$$\begin{aligned} N(\gamma)\,d\gamma &= N_o \left(\gamma^2 - 1\right)^{-(\mu+1)/2} \gamma\,d\gamma\,, \\ &\approx N_o \gamma^{-\mu}\,d\gamma\,, \qquad \gamma \gg 1\,. \end{aligned} \tag{38}$$

The energy spectrum is given by $N(E)\,dE = N(\gamma)\,d\gamma$, with $E = \gamma mc^2$. Thus, the energy spectrum for the shock acceleration of relativistic particles is also expected to be a power-law.

For shock acceleration, the exponent is

$$\mu = \frac{C+2}{C-1}\,, \tag{39}$$

where C is the shock compression (eq. 27 & 29). Strong shocks give $C = 4$ and $\mu = 2$, which is in reasonable agreement with the radio observations of supernova remnants. Merger shocks have $C \approx 2 - 3$, which leads to $\mu \approx 4{-}2.5$. Thus, the particle spectra produced by merger shocks are expected to be significantly steeper than those generated by supernova remnant blast waves.

5.2.2 Reacceleration by Merger Shocks. Merger shocks may reaccelerate pre-existing relativistic particles, rather than produce new particles from the thermal ICM. This mechanism has been proposed to explain the radio halo in the Coma cluster and other halos (Brunetti et al. 2001a,b). In this model, the reacceleration occurs gradually over an extended period of time.

Radio relics might also be due to the reacceleration of relatistic particles injected as some time in the past by radio galaxies (Enßlin & Brüggen 2001). In this case, one would only expect to see relics associated with a small fraction of merger shocks; one would require both a merger shock and a pre-existing radio population. If the old radio plasma continues to be separated from the thermal plasma (a radio "ghost," Enßlin 2001), then the merger shock will be subsonic in the relativistic radio plasma. Thus, rather than reacceleration, the merger shock might re-energize the radio plasma by adiabatic compression.

5.2.3 Turbulent Acceleration Following a Merger. Cluster mergers may produce a significant level of turbulence in the ICM, and this could lead to turbulent acceleration or reacceleration of relativistic electrons (Eilek & Weatherall 1999). This is second order Fermi acceleration. Turbulent reacceleration has been suggested to explain radio halos in clusters (Brunetti et al. 2001a,b). Radio halos have only been found in merging clusters. However, their smooth distributions and central locations suggest that they are not confined to the region currently passing through a merger shock. Turbulent acceleration following the passage of merger shocks might explain these properties.

5.2.4 Secondary Electron Production. Another source of relativistic electrons is the decay of charged mesons generated in cosmic ray ion collisions (Dennison 1980; Vestrand 1982; Colafrancesco & Blasi 1998). The reactions involved are

$$\begin{aligned} p + p &\rightarrow \pi^{\pm} + X\,, \\ \pi^{\pm} &\rightarrow \mu^{\pm} + \nu_{\mu}\,(\bar{\nu}_{\mu}) \\ \mu^{\pm} &\rightarrow e^{\pm} + \bar{\nu}_{\mu}\,(\nu_{\mu}) + \nu_{e}\,(\bar{\nu}_{e})\,. \end{aligned} \tag{40}$$

Here, X represents some combination of protons, neutrons, and/or other particles. The electrons (and positrons) produced by this mechanism are referred to as secondary electrons. If the primary cosmic ray ions are due to AGNs or star bursts, this process might have no connection with cluster mergers. On the other hand, the ions might have been accelerated or reaccelerated by cluster merger shocks or turbulence associated with cluster mergers. Recently, Enßlin (2001) proposed that primary ions in clusters were originally produced by AGN or starbursts, but had lost most of their energy due to adiabatic losses. He argued that these ions are reaccelerated by merger shocks, and the subsequent secondary electrons make cluster radio halos.

5.3. MODELS FOR MERGER SHOCKS AND PRIMARY ELECTRONS

Here, I describe the results of some models for the population of relativistic electrons in clusters, assuming they are primary electrons accelerated in merger shocks (Sarazin 1999a; § 5.2.1). The populations of cosmic ray electrons in clusters depends on their merger histories. Because low energy electrons have long lifetimes, one expects to find a large population of them in most clusters (any cluster which has had a significant merger since $z \sim 1$). On the other hand, higher energy electrons ($E \gtrsim 1$ GeV) have short lifetimes (shorter than the time for a merger shock to cross a cluster). Thus, one only expects to find large numbers of higher energy primary electrons in clusters which are having or have just had a merger. These conclusions follow from a large number of detailed models of the evolution of the integrated electron population in clusters (Sarazin 1999a). Two recent cluster merger simulations have included particle acceleration approximately (Roettiger, Burns, & Stone 1999; Takizawa & Naito 2000), and they reach similar conclusions.

Figure 1.7 shows the electron spectrum in a cluster with a typical history. Most of the electron energy is in electrons with $\gamma \sim 300$, which have the longest lifetimes. These electrons are produced by mergers over the entire history of the cluster. This cluster also has a small ongoing merger which produces the high energy tail on the electron distribution. In cluster models without a current merger, the high energy tail would be missing.

Most of the emission from these electrons is due to IC, and the resulting spectrum is shown in Figure 1.8. For comparison, thermal bremsstrahlung with a typical rich cluster temperature and luminosity is shown as a dashed curve. Figure 1.8 shows that clusters should be strong sources of extreme ultraviolet (EUV) radiation. Since this emis-

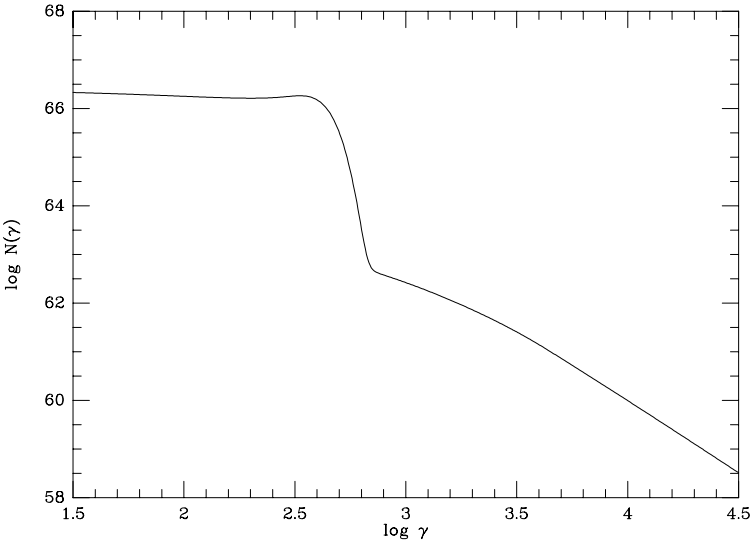

Figure 1.7. A typical model for the relativistic electron population in a cluster of galaxies. The lower energy electrons are due to all of the mergers in the cluster history, while the high energy electrons are due to a small current merger.

sion is due to electrons with $\gamma \sim 300$ which have very long lifetimes, EUV radiation should be a common feature of clusters (Sarazin & Lieu 1998).

In clusters with an ongoing merger, the higher energy electrons will produce a hard X-ray tail via IC scattering of the Cosmic Microwave Background (CMB); the same electrons will produce diffuse radio synchrotron emission.

5.4. NONTHERMAL EMISSION AND MERGERS

5.4.1 Radio Halos and Relics . The oldest and most detailed evidence for nonthermal populations in clusters comes from the radio. A number of clusters of galaxies are known to contain large-scale diffuse radio sources which have no obvious connection to individual galaxies in the cluster (Giovannini et al. 1993). These sources are referred to as radio halos when they appear projected on the center of the cluster, and are called relics when they are found on the cluster periphery (although they have other distinctive properties). In all cases of which I am aware, they have been found in clusters which show significant evidence for an ongoing merger (Giovannini et al. 1993; Feretti 1999; Feretti 2000). Since these source are discussed extensively in another chapter of this

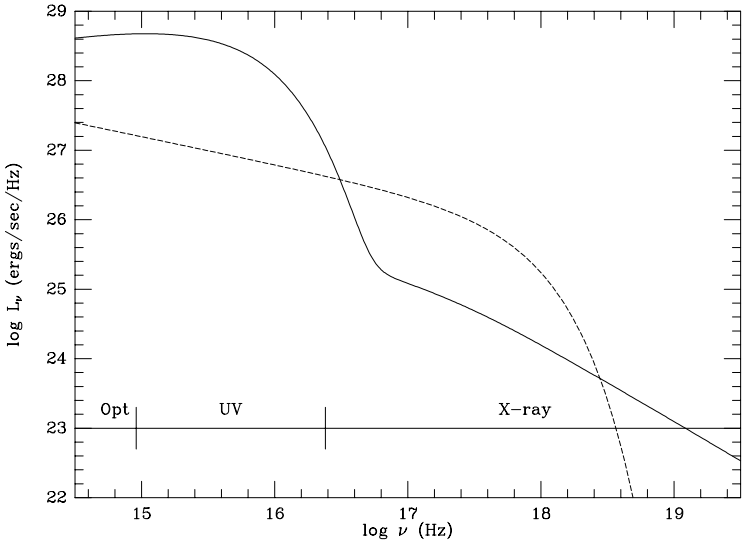

Figure 1.8. The IC spectrum from a typical cluster model (solid curve). This is the same model as shown in Figure 1.7. The dashed curve is a 7 keV thermal bremsstrahlung spectrum.

book (Giovannini & Feretti 2001), I won't discuss them in any more detail here.

5.4.2 EUV/Soft X-ray Emission. Excess EUV emission has apparently been detected with the EUVE satellite in six clusters (Virgo, Coma, Abell 1795, Abell 2199, Abell 4038, & Abell 4059; Lieu et al. 1996a,b; Bowyer & Berghöfer 1998; Mittaz, Lieu, & Lockman 1998; Bowyer, Berghöfer, & Korpela 1999; Kaastra et al. 1999; Lieu et al. 1999a,b; Berghöfer, Bowyer, & Korpela 2000a,b; Bonamente, Lieu, & Mittaz 2000). In fact, the EUVE satellite appears to have detected all of the clusters it observed which are nearby, which have long integration times, and which lie in directions of low Galactic column where detection is possible at these energies. However, the EUV detections and claimed properties of the clusters remain quite controversial (Bowyer & Berghöfer 1998; Arabadjis & Bregman 1999; Bowyer et al. 1999; Berghöfer et al. 2000a). The EUV observations suggest that rich clusters generally have EUV luminosities of $\sim 10^{44}$ ergs/s, and have spectra which decline rapidly in going from the EUV to the X-ray band.

While it is possible that the EUV emission may be thermal in origin (Fabian 1997; Bonamente et al. 2000), I believe that it is more likely that this emission is due to inverse Compton scattering (IC) of CMB photons by low energy relativistic electrons (Hwang 1997; Bowyer & Berghöfer

1998; Enßlin & Biermann 1998; Sarazin & Lieu 1998). In this model, the EUV would be produced by electrons with energies of ∼150 MeV ($\gamma \sim 300$; Fig. 1.7). As noted above, these electrons have lifetimes which are comparable to the Hubble time, and should be present in essentially all clusters. In fact, many of the clusters with observed EUV emission do not appear to be undergoing mergers at present. Thus, this emission is not a useful diagnostic for an ongoing merger; instead, it may represent the emission from electrons accelerated in many previous mergers. To produce the EUV luminosities observed, one needs a population of such electrons with a total energy of $\sim 10^{62}$ ergs, which is about 3% of the typical thermal energy content of clusters. This is a reasonable acceleration efficiency for these particles, given that both the thermal energy in the intracluster gas and the relativistic particles result from merger shocks. The steep spectrum in going from EUV to X-ray bands is predicted by this model (Fig. 1.8); it results from the rapid increase in losses ($\propto \gamma^2$) for particles as the energy increases above $\gamma \sim 300$ (Figs. 1.5 & 1.6).

5.4.3 Hard X-ray Tails. If clusters contain higher energy relativistic electrons with $\gamma \sim 10^4$, these particles will produce hard X-ray emission by IC scattering. These are essentially the same electrons which produce the observed radio halos and relics (§ 5.4.1), although the detailed correspondence depends on the value of the magnetic field. The ratio of hard X-ray IC emission to radio synchrotron emission allows one to determine the magnetic field in clusters (e.g., Rephaeli 1979; Fusco-Femiano et al. 1999). Since these higher energy electrons have short lifetimes, they should only be present in clusters with evidence for a recent or ongoing merger.

Because of the short lifetimes of the electrons producing HXR IC emission, the population of these particles should be close to steady-state. If the accelerated electrons have a power-law distribution (eq. 39), the expected steady-state energy spectral index if IC losses dominated would be $\alpha_{\rm HXR} = -(\mu + 1)/2$ (Ginzburg & Syrovatskii 1964). For $\mu \approx 2.5 - 4$ (the values expected for typical merger shock compressions), this gives $\alpha_{\rm HXR} \approx -1.75$ to -2.5. In the numerical models, the best-fit spectral indices from 20 to 100 keV are flatter than this, $\alpha_{\rm HXR} \approx -1.1$, mainly because other loss processes are important at the lower energy end of the HXR band (Fig. 1.5).

If the population of high energy electrons is in steady state, the HXR luminosity is just proportional to the energy input from the mergers into high energy electrons. To a good approximation, the present day value of $L_{\rm HXR}$ (20–100 keV) is simply given by

$$L_{\rm HXR} \approx 0.17 \dot{E}_{\rm CR,e}(\gamma > 5000)\,. \qquad (41)$$

where $\dot{E}_{\rm CR,e}(\gamma > 5000)$ is the total present rate of injection of energy in cosmic ray electrons with $\gamma > 5000$. The best-fit coefficient (0.17 in eqn. 41) depends somewhat on the power-law index of the injected electrons; the value of 0.17 applies for $\mu = 2.3$. Assuming a fixed efficiency $\epsilon_{\rm CR,e}(\gamma > 5000)$ of conversion of shock energy into high energy electrons, the rate of particle acceleration is given by

$$\dot{E}_{\rm CR,e}(\gamma > 5000) = \epsilon_{\rm CR,e}(\gamma > 5000)\, \dot{E}_s \,, \tag{42}$$

where $\dot{E}_s$ is the total rate of merger shock energy dissipation. This gives $L_{\rm HXR} \propto \dot{E}_s$.

Hard X-ray emission in excess of the thermal emission and detected as a nonthermal tail at energies $\gtrsim$20 keV has been seen in at least two clusters. The Coma cluster, which is undergoing at least one merger and which has a radio halo, was detected with both BeppoSAX and RXTE (Fusco-Femiano et al. 1999; Rephaeli, Gruber, & Blanco 1999). BeppoSAX has also detected Abell 2256 (Fusco-Femiano et al. 2000), another merger cluster with strong diffuse radio emission. BeppoSAX may have detected Abell 2199 (Kaastra et al. 1999), although I believe the evidence is less compelling for this case. A nonthermal hard X-ray detection of Abell 2199 would be surprising, as this cluster is very relaxed and has no radio halo or relic (Kempner & Sarazin 2000).

An alternative explanation of the hard X-ray tails is that they might be due to nonthermal bremsstrahlung (Blasi 2000; Dogiel 2000; Sarazin & Kempner 2000), which is bremsstrahlung from nonthermal electrons with energies of 10–1000 keV which are being accelerated to higher energies. The nonthermal tail on the particle distribution might also be associated with shock acceleration. On the other hand, these suprathermal electrons have relatively short time scales to relax into the thermal distribution as a result of Coulomb collisions. In fact, this is a general problem of the injection of thermal electrons into the shock acceleration region. IC emission from high energy electrons dominates unless the particle spectrum is very steep (Sarazin & Kempner 2000).

The previous hard X-ray detections of clusters have been done with instruments with very poor angular resolution. Thus, they provide no information on the distribution of the hard X-ray emission. It would be very useful to determine if the hard X-ray emission is localized to the radio emitting regions in clusters. For clusters with radio relics, these might be associated with the positions of merger shocks in the X-ray images. Better angular resolution would also insure that the hard X-ray detections of clusters are not contaminated by emission from other sources. The IBIS instrument on INTEGRAL will provide a hard X-ray

capability with better angular resolution, and may allow the hard X-ray emission regions to be imaged (Goldoni et al. 2001).

The predicted IC emission from nonthermal particles is much weaker than the thermal emission in the central portion of the X-ray band from about 0.3 keV to 20 keV (Fig. 1.8). However, if the IC emission is localized to merger shock regions, its local surface brightness might be comparable to the thermal X-ray emission. A possible detection of localized IC emission associated with merger shocks and radio relics has been claimed in Abell 85 (Bagchi, Pislar, & Lima Neto 1998). It is possible that Chandra and XMM/Newton will find IC emission associated with other merger shocks and radio relics.

5.4.4 Predicted Gamma-Ray and Neutrino Emission.

Relativistic electrons and ions in clusters are also expected to produce strong gamma-ray emission (Dar & Shaviv 1996; Berezinsky et al. 1997; Colafrancesco & Blasi 1998; Blasi & Colafrancesco 1999; Blasi 1999; Sarazin 1999b) The region near 100 MeV is particularly interesting, as this region includes bremsstrahlung from the most common electrons with $\gamma \sim 300$, and π^o decay gamma-rays from ions. The π^o emission mechanism starts with the essentially the same ion-ion collisions as make secondary electrons (eq. 40)

$$\begin{aligned} p + p &\rightarrow \pi^o + X\,, \\ \pi^o &\rightarrow 2\gamma\,. \end{aligned} \tag{43}$$

Both bremsstrahlung and the π^o decay process involve collisions between relativistic particles (electrons for bremsstrahlung, ions for π^o emission) and thermal particles, so they should both vary in the same way with density in the cluster. Thus, the ratio of these two spectrally distinguishable emission processes should tell us the ratio of cosmic ray ions to electrons in clusters (Blasi 1999; Sarazin 1999b).

Figure 1.9 shows the predicted gamma-ray spectrum for the Coma cluster, based on a model which reproduces the observed EUV, hard X-ray, and radio emission (Sarazin 1999b). The observed upper limit from CGO/EGRET is $<4 \times 10^{-8}$ cts/cm^2/s for $E > 100$ MeV (Sreekumar et al. 1996), while the predicted value for this model is $\sim 2 \times 10^{-8}$ cts/cm^2/s. The EGRET upper limit already shows that the ratio of ions to electrons cannot be too large ($\lesssim$30; Blasi 1999; Sarazin 1999b). The predicted fluxes are such that many nearby clusters should be easily detectable with GLAST.

The same relativistic particles will also produce neutrinos, which might be detectable with future instruments (Dar & Shaviv 1996; Berezinsky et al. 1997; Colafrancesco & Blasi 1998).

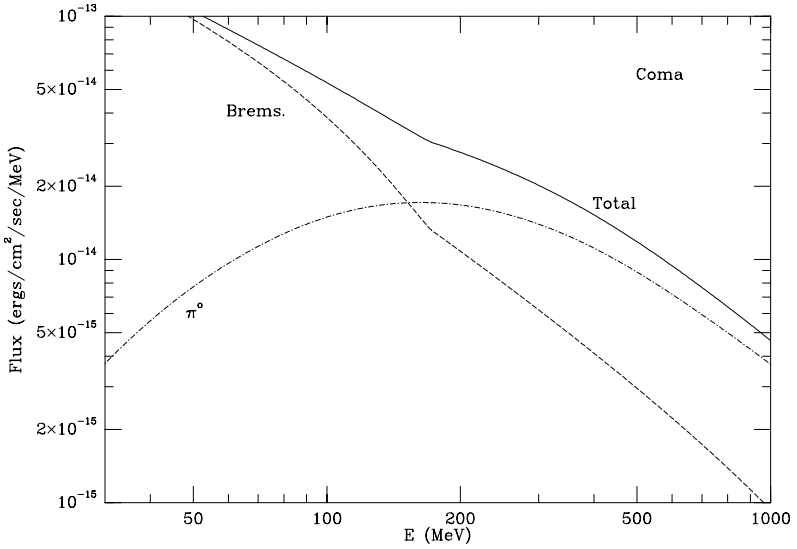

Figure 1.9. The predicted gamma-ray spectrum for the Coma cluster, including electron bremsstrahlung and π^o decay from ions (Sarazin 1999b).

5.4.5 Ultra High Energy Cosmic Rays. The time scale for most relativistic particles to diffuse out of clusters is longer than the Hubble time (eq. 35). However, very high energy cosmic rays ($E \gtrsim 10^{15}$ eV) could escape from clusters on relatively short time scales. In the cosmic ray spectrum seen at the Earth, it is believed that particles with energies up to $\sim 10^{14}$ eV come from supernova explosions in our Galaxy. Other Galactic sources may produce even higher energy cosmic rays. However, it is likely that the highest energy cosmic ray particles ($E \gtrsim 3 \times 10^{18}$ eV) are extragalactic in origin (Cocconi 1956). Merger or accretion shocks in clusters of galaxies are a possible source of such particles (e.g., Kang et al. 1996,1997; Siemieniec-Oziębło & Ostrowski 2000). The advantages of merger shocks are their high total energies (which helps with the overall flux of cosmic rays), their very large physical sizes (which help with the acceleration of high energy particles with large Larmor radii), their long time scales (which helps to provide enough time for the particles to diffuse to these high energies), and the relatively low losses in the cluster environment (§ 5.1). The Larmor or gyro radius of a high energy particle with a charge Z in the ICM is

$$r_g = \frac{pc}{ZeB} \approx \frac{0.1}{Z} \left(\frac{E}{10^{20}\,\mathrm{eV}} \right) \left(\frac{B}{1\,\mu\mathrm{G}} \right)^{-1} \mathrm{Mpc}\,, \tag{44}$$

and cluster shock regions are likely to be about this size or larger. Assuming Bohm diffusion and a strong shock at a velocity v_s, the acceler-

ation time is about (Kang et al. 1996)

$$t_{\rm acc} \approx 9 \times 10^9 \left(\frac{E}{10^{20}\,{\rm eV}}\right) \left(\frac{B}{1\,\mu{\rm G}}\right)^{-1} \left(\frac{v_s}{3000\,{\rm km/s}}\right)^{-2} {\rm yr}\,. \qquad (45)$$

Thus, it might be possible to accelerate protons up to $\lesssim 10^{20}$ eV in cluster shocks.

6. SUMMARY

I've tried to summarize some of the basic aspects of the physics of cluster mergers. Simple estimates for the rates of mergers and for the infall velocities and impact parameters were given in § 2. The thermal effects of merger shocks are discussed in § 3, with an emphasis on the diagnostics for determining the kinematics of mergers from X-ray observations of temperatures and densities in the ICM. The interaction of cooling flow cores with hotter, more diffuse intracluster gas was considered in (§ 4), including the mechanism for the disruption of the cooling flow cores (§ 4.1), and the hydrodynamics of "cold fronts" (§ 4.2). Relativistic particles may be accelerated or reaccelerated in merger shocks or turbulence generated by mergers. The nonthermal effects of mergers are discussed in § 5, including the resulting radio, extreme ultraviolet, hard X-ray, and gamma-ray emission.

Acknowledgments

I want to thank my collaborators Josh Kempner, Maxim Markevitch, Scott Randall, Paul Ricker, and Alexey Vikhlinin for all their help. I would like to particularly thank Paul Ricker for useful discussions, and Josh Kempner, Scott Randall, and Yutaka Fujita for careful readings of a draft. Scott Randall and Paul Ricker kindly provided figures for this paper. Support for this work was provided by the National Aeronautics and Space Administration through Chandra Award Numbers GO0-1119X, GO0-1173X, GO0-1158X, and GO1-2122X, issued by the Chandra X-ray Observatory Center, which is operated by the Smithsonian Astrophysical Observatory for and on behalf of NASA under contract NAS8-39073. Support also came from NASA XMM grants NAG 5-10074 and NAG 5-10075.

References

Arabadjis, J. S., & Bregman, J. N. 1999, ApJ, 514, 607

Arnaud, K., Fabian, A., Eales, S., Jones, C., & Forman, W. 1984, MNRAS, 211, 981

Atoyan, A. M., & Völk, H. J. 2000, ApJ, 535, 45

Bagchi, J., Pislar, V., & Lima Neto, G. B. 1998, MNRAS, 296, L23
Bahcall, N. A., & Fan, X. 1998, ApJ, 504, 1
Bardeen, J. M., Bond, J. R., Kaiser, N., & Szalay, A. S. 1986, ApJ, 304, 15
Bell, A. R. 1978, MNRAS, 182, 147
Berezinsky, V. S., Blasi, P., & Ptuskin, V. S. 1997, ApJ, 487, 529
Berghöfer, T. W., Bowyer, S., & Korpela, E. 2000, ApJ, 535, 615
Berghöfer, T. W., Bowyer, S., & Korpela, E. 2000b, ApJ, 545, 695
Blandford, R. D., & Eichler, D. 1987, Phys. Rep., 154, 1
Blandford, R. D., & Ostriker, J. P. 1978, ApJ, 221, L29
Blasi, P. 1999, ApJ, 525, 603
Blasi, P. 2000, ApJ, 532, L9
Blasi, P., & Colafrancesco, S. 1999, APh, 12, 169
Bonamente, M., Lieu, R., & Mittaz, J. 2000, ApJ, in press
Bond, J. R., Cole, S., Efstathiou, G., & Kaiser, N. 1991, ApJ, 379, 440
Bowyer, S., & Berghöfer, T. W. 1998, ApJ, 506, 502
Bowyer, S., Berghöfer, T. W., & Korpela, E. 1999, ApJ, 526, 592
Brunetti, G., Setti, G., Feretti, L., & Giovannini, G. 2001a, MNRAS, 320, 365
Brunetti, G., Setti, G., Feretti, L., & Giovannini, G. 2001b, NewA, 6, 1
Bryan, G. L., & Norman, M. L. 1998, ApJ, 495, 80
Buote, D. A., & Tsai, J. C. 1996, ApJ, 458, 27
Cavaliere, A., Menci, N., & Tozzi, P. 1999, MNRAS, 308, 599
Cocconi, G. 1956, Nuovo Cim., 3, 1433
Colafrancesco, S., & Blasi, P. 1998, APh, 9, 227
Dar, A., & Shaviv, N. J. 1996, Astropart. Phys., 4, 343
Dennison, B. 1980, ApJ, 239, L93
Dogiel, V. A. 2000, A&A, 357, 66
Edge, A. C., Stewart, G. C., & Fabian, A. C. 1992, MNRAS, 258, 177
Eilek, J., & Weatherall, J. 1999, in Proc. Diffuse Thermal and Relativistic Plasma in Galaxy Clusters, ed. H. Böringer, L. Feretti, & P. Schuecker (Garching: MPE), 249
Enßlin, T. A. 2001, preprint
Enßlin, T. A., & Brüggen, M. 2001, MNRAS, in press (astro-ph/0104233)
Enßlin, T. A., & Biermann, P. L. 1998, A&A, 330, 90
Ettori, S., & Fabian, A. C. 2000, MNRAS, 317, L57
Evrard, A. E., & Gioia, I. M. 2001, in Merging Processes in Clusters of Galaxies, ed. L. Feretti, I. M. Gioia, & G. Giovannini (Dordrecht: Kluwer), in press
Fabian, A. C. 1994, ARA&A, 32, 277
Fabian, A. C. 1997, Science, 275, 48
Fabian, A. C., & Daines, S. J. 1991, MNRAS, 252, 17p

Feretti, L. 1999, in Proc. Diffuse Thermal and Relativistic Plasma in Galaxy Clusters, ed. H. Böringer, L. Feretti, & P. Schuecker (Garching: MPE), 1
Feretti, L. 2000, preprint (astro-ph/0006379)
Forman, W. R. 2001, in Merging Processes in Clusters of Galaxies, ed. L. Feretti, I. M. Gioia, & G. Giovannini (Dordrecht: Kluwer), in press
Fusco-Femiano, R., et al., 1999, ApJ, 513, L21
Fusco-Femiano, R., et al., 2000, ApJ, 534, L7
Ginzburg, V. L., & Syrovatskii, S. I. 1964, The Origin of Cosmic Rays
Giovannini, G., et al., 1993, ApJ, 406, 399
Giovannini, G., & Feretti, L. 2001, in Merging Processes in Clusters of Galaxies, ed. L. Feretti, I. M. Gioia, & G. Giovannini (Dordrecht: Kluwer), in press
Goldoni, P., Goldwurm, A., Laurent, P., Casse, M., Paul, J., & Sarazin, C. 2001. in INTEGRAL Science Workshop, in press (astro-ph/0102363)
Gómez, P. L., Loken, C., Roettiger, K., & Burns, J. O. 2001, ApJ, in press.
Guy, T. B. 1974, Amer. Inst. Aero. Astro. J., 12, 380
Henriksen, M. J. 1988, ApJ, 407, L13
Hwang, C.-Y. 1997, Science, 278, 1917
Kaastra, J. S., et al., 1999, ApJ, 519, L119
Kang, H., Rachen, J. P., & Biermann, P. L. 1997, MNRAS, 286, 257
Kang, H., Ryu, D., & Jones, T. W. 1996, ApJ, 456, 422
Kempner, J., & Sarazin, C. L. 2000, ApJ, 530, 282
Kempner, J., Sarazin, C. L., & Ricker, P. R. 2001, preprint
Kitayama, T., & Suto, Y. 1996, ApJ, 469, 480
Lacey, C., & Cole, S. 1993, MNRAS, 262, 627
Landau, L. D., & Lifshitz, E. M. 1959, Fluid Mechanics (Oxford: Pergamon Press)
Lieu, R., et al., 1996b, Science, 274, 1335
Lieu, R., et al., 1996b, ApJ, 458, L5
Lieu, R., Bonamente, M., & Mittaz, J. 1999a, ApJ, 517, L91
Lieu, R., et al., 1999, ApJ, 527, L77
Markevitch, M., Forman, W. R., Sarazin, C. L., & Vikhlinin, A. 1998, ApJ, 503, 77
Markevitch, M., Sarazin, C. L., & Vikhlinin, A. 1999, ApJ, 521, 526
Markevitch, M., et al., 2000, ApJ, 541, 542
Markevitch, M., Vikhlinin, A., Mazzotta, P., & Van Speybroeck, L. 2001, in X-ray Astronomy 2000, ed. R. Giacconi, L. Stella, & S. Serio (San Francisco: ASP), in press (astro-ph/0012215)
Mazzotta, P., Markevitch, M., Vikhlinin, A., Forman, W. R., David, L. P., & Van Speybroeck, L. 2001, ApJ, in press (astro-ph/0102291)

McGlynn, T. A., & Fabian, A. C. 1984, MNRAS, 208, 709
Mittaz, J. P. D., Lieu, R., & Lockman, F. J. 1998, ApJ, 498, L17
Moekel. W. E. 1949, Approximate Method for Predicting Forms and Location of Detached Shock Waves Ahead of Plane or Axially Symmetric Bodies, NACA Technical Note 1921
Navarro, J. F., Frenk, C. S., & White, S. D. M. 1997, ApJ, 490, 493
Owen, F. N., Ledlow, M. J., Morrison, G. E., & Hill, J. M. 1997, ApJ, 488, L15
Peebles, P. J. E. 1969, ApJ, 155, 393
Peebles P. J. E. 1980, The Large-Scale Structure of the Universe (Princeton: Princeton Univ. Press)
Press, W. H., & Schechter, P. 1974, ApJ, 187, 425
Radvogin, Y. B. 1974, Sov. Phys. Dokl., 19, 179
Randall, S. W., & Sarazin, C. L. 2001, preprint
Rephaeli, Y. 1979, ApJ, 227, 364
Rephaeli, Y., Gruber, D., & Blanco, P. 1999, ApJ, 511, L21
Ricker, P. M., & Sarazin, C. L. 2001, preprint
Roettiger, K., Burns, J., & Stone, J. M. 1999, ApJ, 518, 603
Roettiger, K., Stone, J. M., & Burns, J. 1999, ApJ, 518, 594
Rusanov, V. V. 1976, Ann. Rev. Fluid Mech., 8, 377
Sarazin, C. L. 1999a, ApJ, 520, 529
Sarazin, C. L. 1999b, in Proc. Diffuse Thermal and Relativistic Plasma in Galaxy Clusters, ed. H. Böringer, L. Feretti, & P. Schuecker (Garching: MPE), 185
Sarazin, C. L., & Kempner, J. 2000, ApJ, 533, 73
Sarazin, C. L., & Lieu, R. 1998, ApJ, 494, L177
Schindler, S. 2001, in Merging Processes in Clusters of Galaxies, ed. L. Feretti, I. M. Gioia, & G. Giovannini (Dordrecht: Kluwer), in press
Schindler, S., & Müller E. 1993, A&A, 272, 137
Schreier, S. 1982, Compressible Flow (New York: Wiley), 182-189
Siemieniec-Oziębło, G., & Ostrowski, M. 2000, A&A, 355, 51
Spitzer, L. 1962, Physics of Fully Ionized Gases (New York: Wiley),
Sreekumar, P., et al., 1996, ApJ, 464, 628
Sugerman, B., Summers, F. J., & Kamionkowski, M. 2000, MNRAS, 311, 762
Takizawa, M. 1999, ApJ, 520, 514
Takizawa, M. 1999, ApJ, 532, 183
Takizawa, M., & Naito, T. 2000, ApJ, 535, 586
Vestrand, W. T. 1982, AJ, 87, 1266
Vikhlinin, A., Markevitch, M., & Murray, S. M. 2001a, ApJ, 549, L47
Vikhlinin, A., Markevitch, M., & Murray, S. M. 2001b, ApJ, 551, 160
White, S. D. M. 1984, ApJ, 286, 38

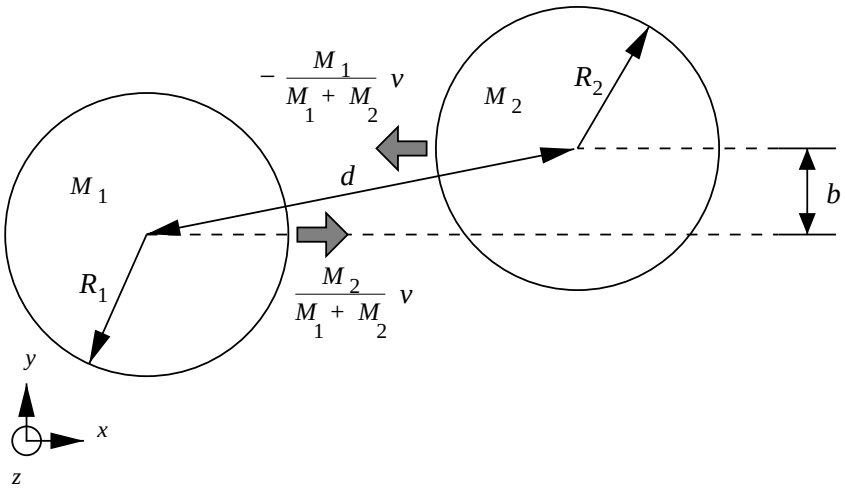
$-\frac{M_1}{M_1+M_2}v$
M_2
R_2
M_1
d
b
R_1
$\frac{M_2}{M_1+M_2}v$
y
x
z

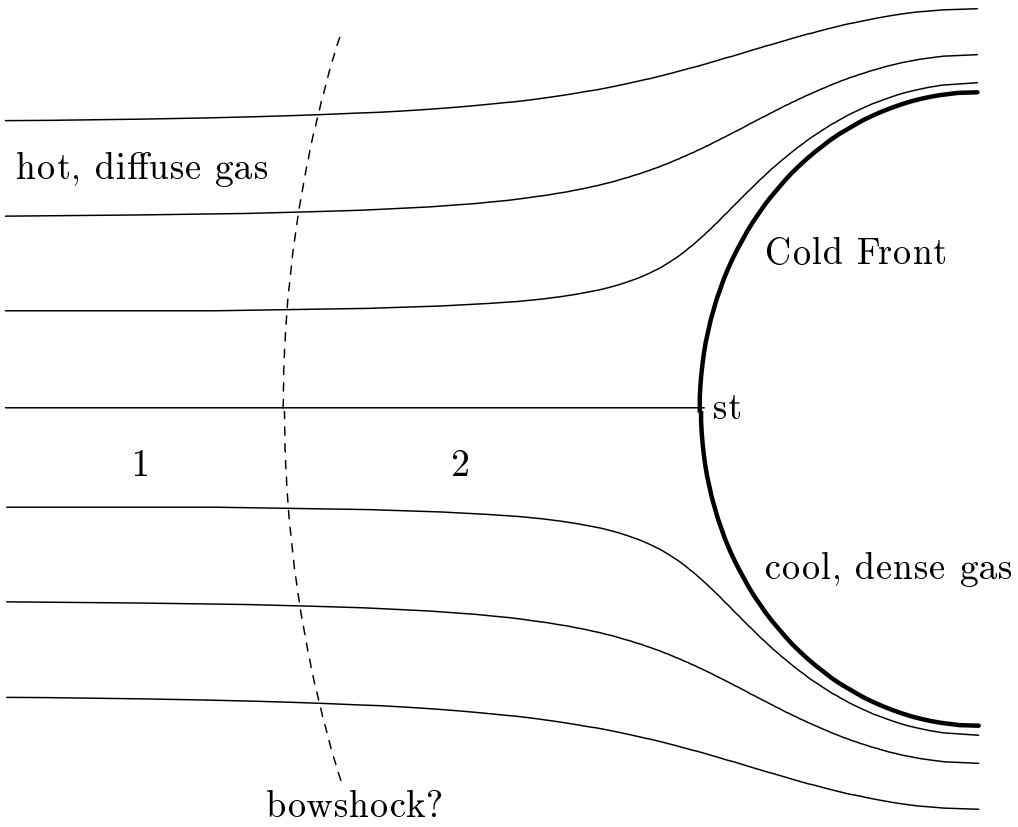
hot, diffuse gas
Cold Front
st
1
2
cool, dense gas
bowshock?

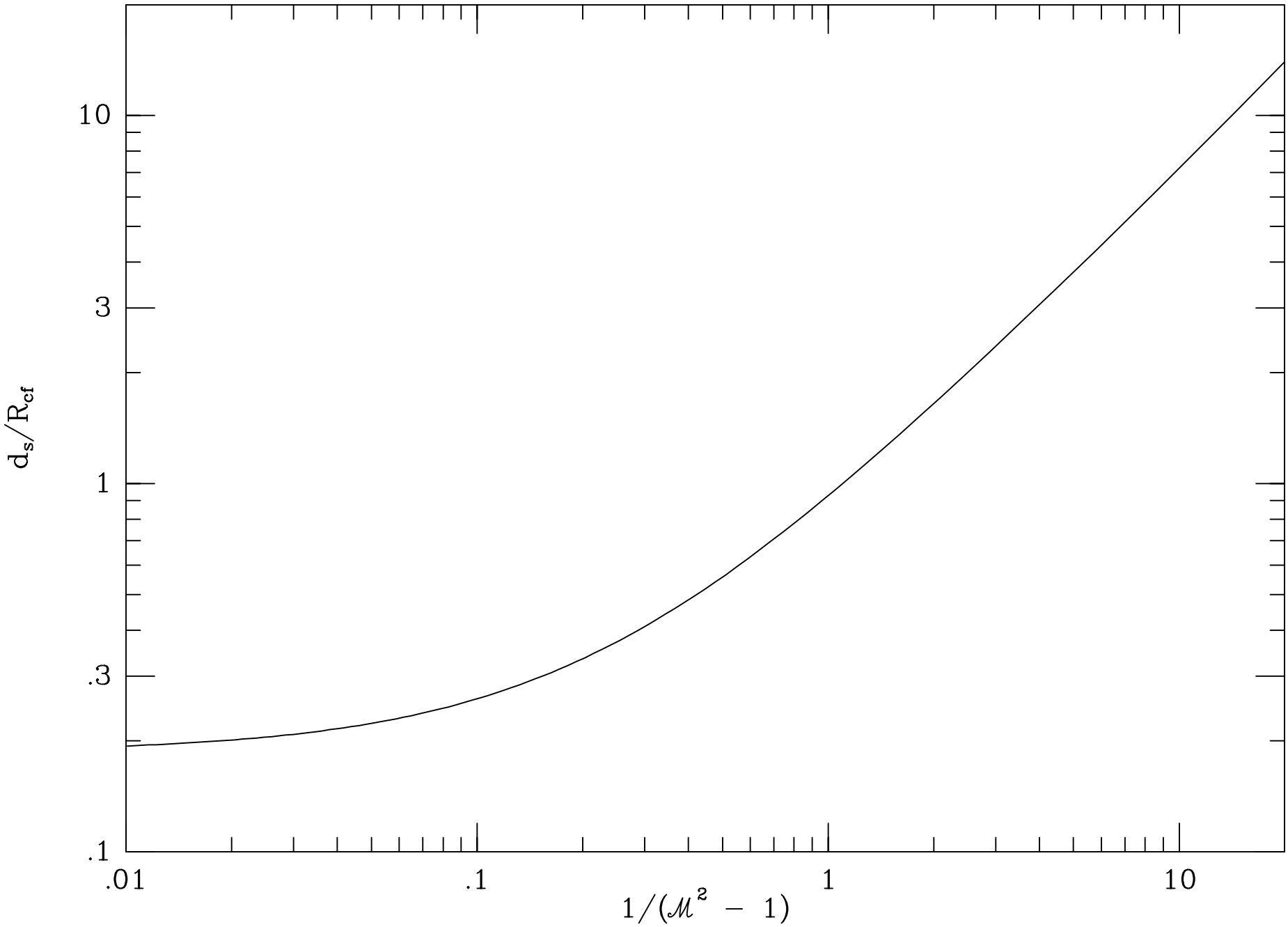
10
3
1
.3
.1
d_s/R_{cf}
.01
.1
1
10
$1/(\mathcal{M}^2 - 1)$

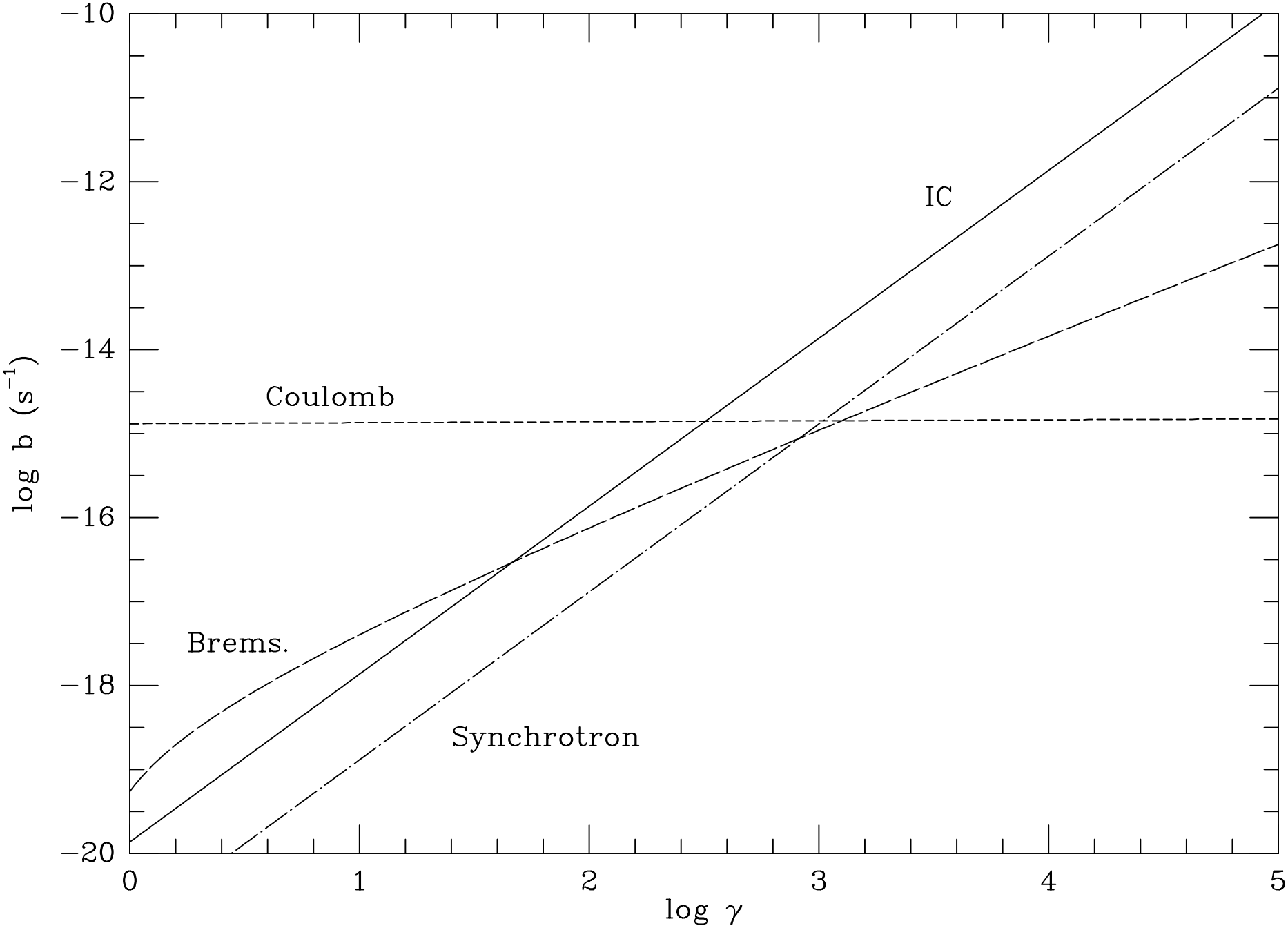
−10
−12
−14
−16
−18
−20
log b (s^{-1})
0
1
2
3
4
5
log γ
IC
Coulomb
Brems.
Synchrotron

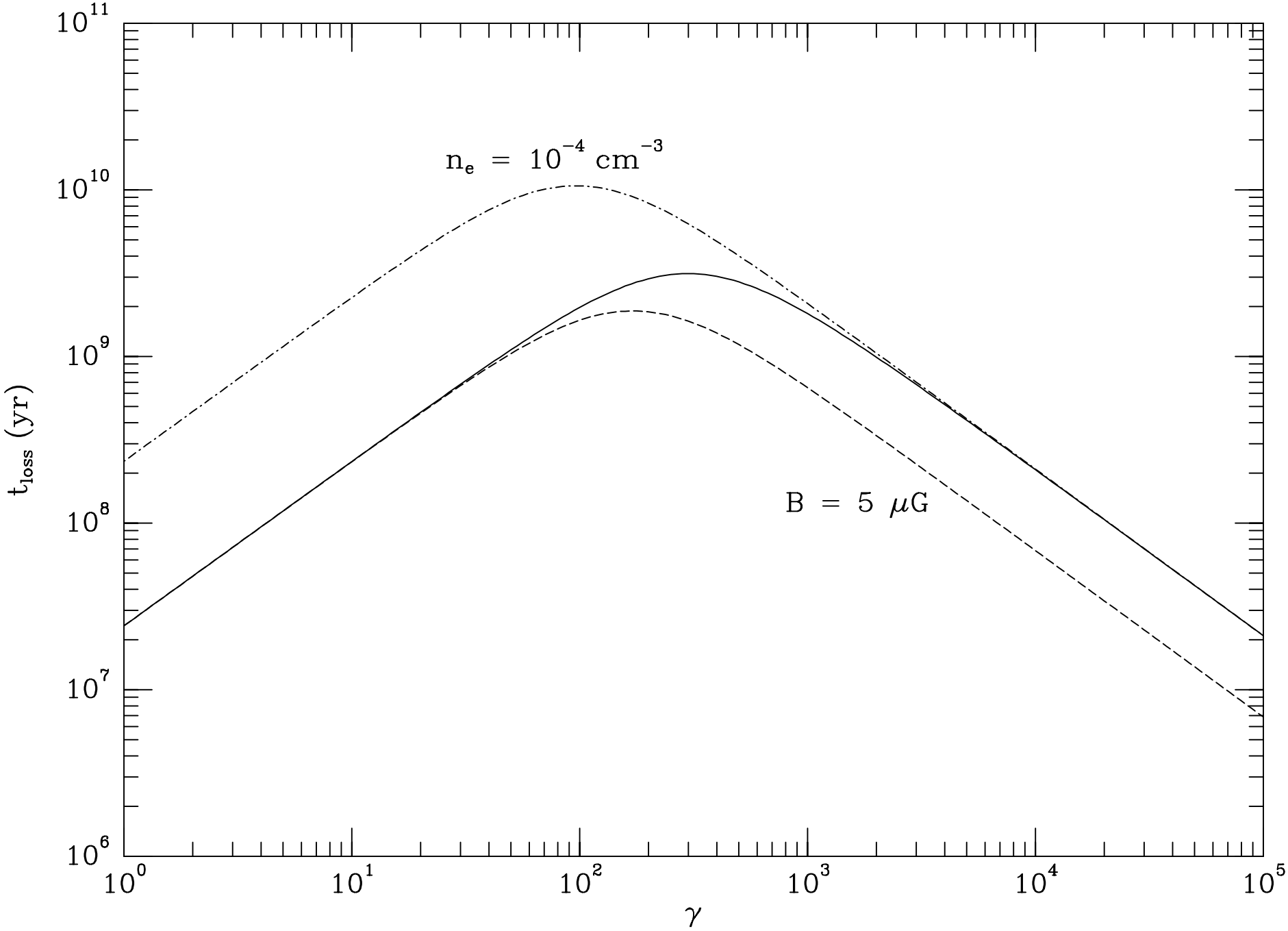
10^{11}
10^{10}
10^{9}
10^{8}
10^{7}
10^{6}
t_{loss} (yr)
$n_e = 10^{-4}$ cm^{-3}
B = 5 μG
10^{0}
10^{1}
10^{2}
10^{3}
10^{4}
10^{5}
γ

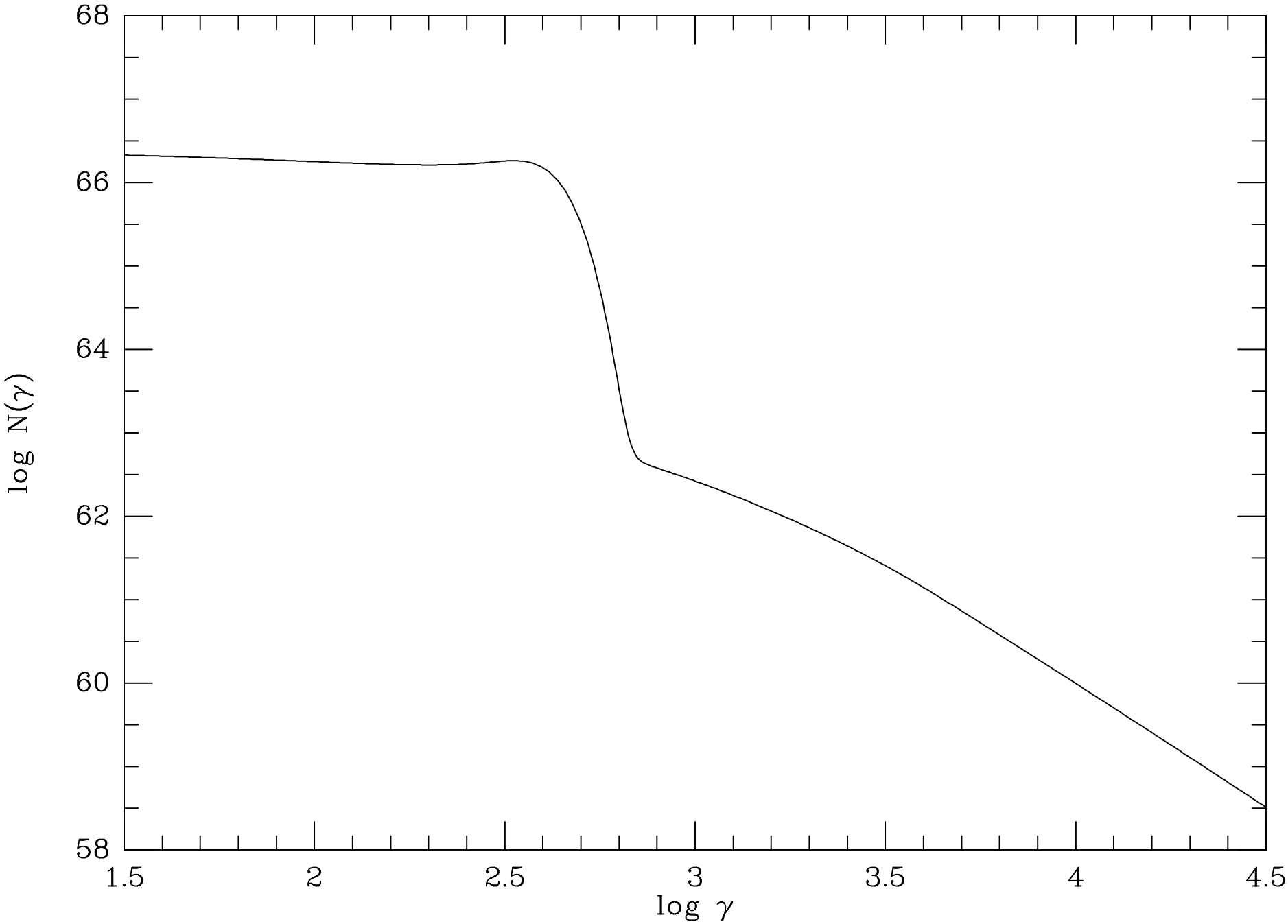
68
66
64
62
60
58
log N(γ)
1.5
2
2.5
3
3.5
4
4.5
log γ

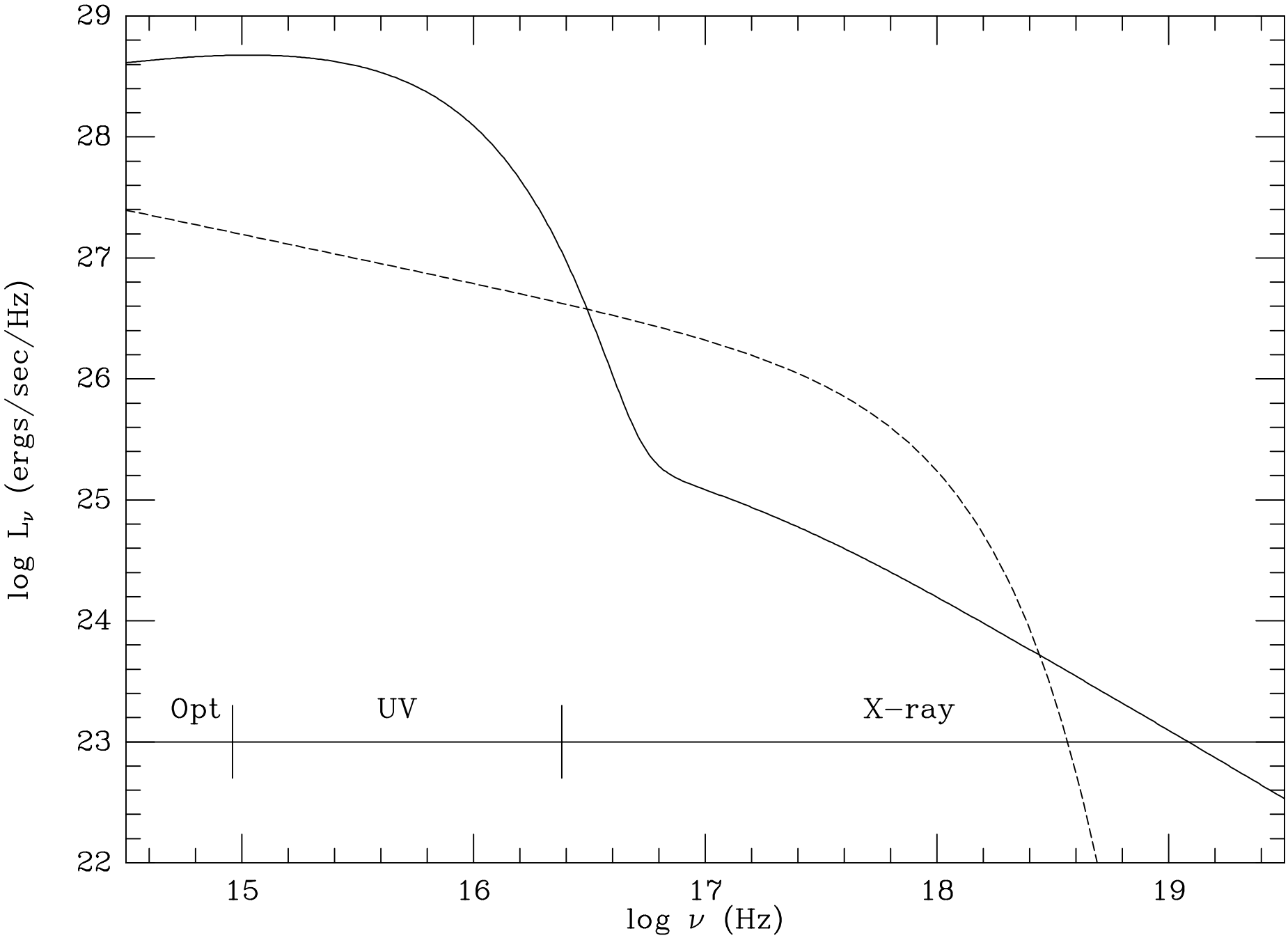
29
28
27
26
25
24
23
22
log L_ν (ergs/sec/Hz)
Opt
UV
X−ray
15
16
17
18
19
log ν (Hz)

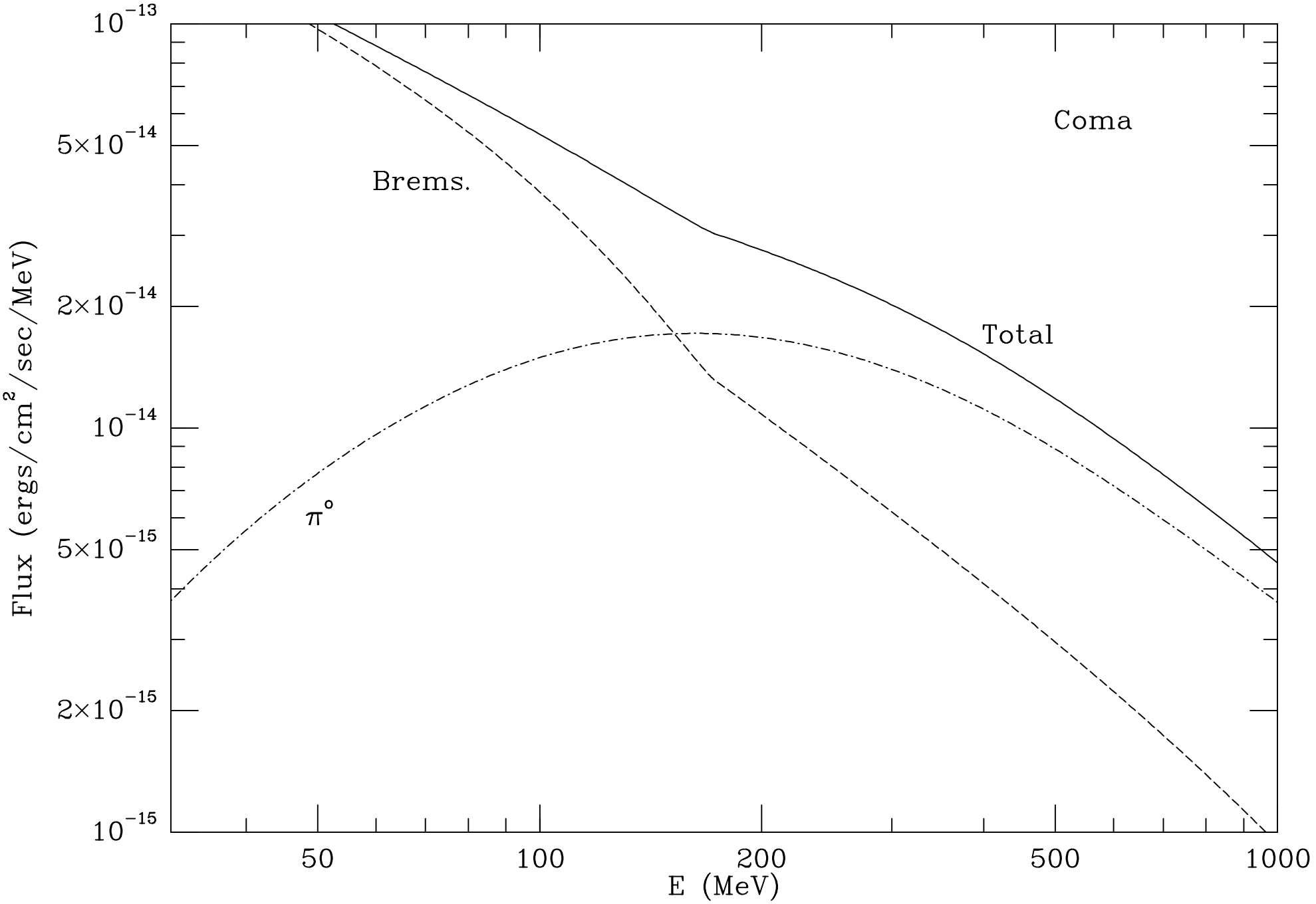
Coma
Brems.
Total
π°
Flux (ergs/cm²/sec/MeV)
E (MeV)
10⁻¹³
5×10⁻¹⁴
2×10⁻¹⁴
10⁻¹⁴
5×10⁻¹⁵
2×10⁻¹⁵
10⁻¹⁵
50
100
200
500
1000